



1 **Modeling of PAHs From Global to Regional Scales:**
2 **Model Development and Investigation of Health Risks**
3 **from 2013 to 2018 in China**

4 Zichen Wu^{1,2,3}, Xueshun Chen^{1,2,3*}, Zifa Wang^{1,2,3*}, Huansheng Chen^{1,2,3}, Zhe
5 Wang^{1,2,3}, Qing Mu⁴, Lin Wu^{1,2,3}, Wending Wang^{1,2,3}, Xiao Tang^{1,2,3}, Jie Li^{1,2,3}, Ying
6 Li^{1,2,3}, Qizhong Wu⁵, Yang Wang^{3,6}, Zhiyin Zou^{1,2,3}, Zijian Jiang^{1,2,3}

7 ¹ State Key Laboratory of Atmospheric Boundary Layer Physics and Atmospheric Chemistry, Institute
8 of Atmospheric Physics, Chinese Academy of Sciences, Beijing 100029, China

9 ² Key Laboratory of Atmospheric Environment and Extreme Meteorology, Institute of Atmospheric
10 Physics, Chinese Academy of Sciences, Beijing 100029, China

11 ³ University of Chinese Academy of Sciences, Beijing 100049, China

12 ⁴ Department of Health and Environmental Sciences, School of Science, Xi'an Jiaotong-Liverpool
13 University, Suzhou 215123, China

14 ⁵ Beijing Normal University, Beijing 100875, China

15 ⁶ Research Center for Eco-Environmental Sciences, Chinese Academy of Sciences, Beijing 100085,
16 China

17 *Correspondence to:* Xueshun Chen (chenxsh@mail.iap.ac.cn) and Zifa Wang (zifawang@mail.iap.ac.cn)

18 **Abstract.** Polycyclic aromatic hydrocarbons (PAHs) significantly impact human health due to their
19 persistence, toxicity, and potential carcinogenicity. Their global distribution and regional changes caused
20 by emission changes, especially over areas in developing countries, remain to be understood along with
21 their health impacts. This study implemented a PAH module in the global-regional nested Atmospheric
22 Aerosol and Chemistry Model (IAP-AACM) to investigate the global distribution of PAHs and the
23 change in their health risks from 2013 to 2018 in China. An evaluation against observations showed that
24 the model could capture well the spatial distribution and seasonal variation of Benzo[a]pyrene (BaP), the
25 typical indicator species of PAHs. At a global scale, the annual mean concentrations are highest in China,
26 followed by Europe and India, with high values exceeding the target values of 1 ng m⁻³ over some areas.
27 Compared with 2013, the concentration of BaP in China decreased in 2018 due to emission reductions,
28 whereas it increased in India and Southern Africa. However, the decline is much smaller than for PM_{2.5}
29 during the same period. The concentration of BaP decreased by 8.5% in Beijing-Tianjin-Hebei (BTH)
30 and 9.4% in the Yangtze River Delta (YRD). It even increased over areas in the Sichuan Basin due to
31 changes in meteorological conditions. The total incremental lifetime cancer risk (ILCR) posed by BaP



32 only showed a slight decrease in 2018 and the population in East China still faced significant potential
33 health risks. The results indicate that strict additional control measures should be taken to reduce the
34 pollution and health risks of PAHs effectively. The study also highlights the importance of considering
35 changes in meteorological conditions when evaluating emission changes from concentration monitoring.

36 **1 Introduction**

37 Polycyclic aromatic hydrocarbons (PAHs) are aromatic compounds with two or more aromatic rings.
38 PAHs have been categorized as persistent organic pollutants (POPs) by the United Nations Economic
39 Commission for Europe's (UNECE's) Convention on Long-Range Transboundary Air Pollution
40 (CLRTAP) (Friedman and Selin, 2012), and they are widely distributed in the environment through
41 atmospheric transport. PAHs have attracted significant attention in environmental research and risk
42 assessment due to their persistence, toxicity, and potential carcinogenicity (Chen and Liao, 2006; Shen
43 et al., 2014). These compounds are generated from both natural and anthropogenic sources (Haritash and
44 Kaushik, 2009). Volcanic eruption, forest, and prairie fire are the major natural sources of atmospheric
45 PAHs (Baek et al., 1991). Anthropogenic sources are the most important source of PAHs, including
46 incomplete combustion of fossil fuels and biomass (Li et al., 2022; Ravindra et al., 2008).

47 Understanding the sources, distribution, and fate of PAHs is crucial for assessing their impacts on
48 human health and the environment. Upon emission into the atmosphere, PAHs are redistributed by gas-
49 particulate partitioning, gaseous-phase reactions, heterogeneous reactions, air-soil exchange, and wet/dry
50 deposition during long-range transport (LRT, Inomata et al., 2013). Monitoring is the most commonly
51 used way to investigate the concentration of PAHs in the atmosphere. Due to the high costs of observation
52 and technical limitations, it is difficult to conduct a long-term and broad regional analysis through
53 monitoring (Zhen, 2023). Up to now, there are few continuous observations over the major continents at
54 the same time (Dong et al., 2023). A transport model is an effective tool to simulate the distribution of
55 PAHs and their LRT, which can greatly enhance our understanding of the distribution of PAHs on a
56 regional and global scale (Byun and Schere, 2006; Wang et al., 2021).

57 As recently outlined by Galarneau et al. (2014), several numerical modeling studies have been
58 reported in the literature. The models that can simulate PAHs include but are not limited to the following
59 examples, GEOS-Chem (Friedman et al., 2014; Friedman and Selin, 2012), ECHAM5 (Lammel and



60 Sehili, 2007; Lammel et al., 2009; Lammel et al., 2015; Octaviani et al., 2019), CAM5 (Lou et al., 2023;
61 Shrivastava et al., 2017), and MOZART-4 (Shen et al., 2014). The horizontal resolutions of these reported
62 models are primarily at $4^\circ \times 5^\circ$ and $2.8^\circ \times 2.8^\circ$. Shen et al. (2014) simulated the transport of
63 Benzo[a]pyrene (BaP), one of the most toxic and highly carcinogenic PAHs, in the global troposphere
64 based on MOZART-4, and they showed that the model resolution was crucial for the health risks
65 assessment. Lammel et al. (2015) demonstrated the significant impact of gas-particle partitioning
66 mechanisms on the atmospheric lifetime, compartment distributions, and LRT of PAHs. The regional
67 modeling studies focusing on Europe, East Asia, and North America have also been reported, with
68 horizontal resolutions ranging mainly from $54 \text{ km} \times 54 \text{ km}$ to $24 \text{ km} \times 24 \text{ km}$ (CMAQ (Aulinger et al.,
69 2009; Aulinger et al., 2007; Bieser et al., 2012; San José et al., 2013; Efsthathiou et al., 2016), WRF-Chem
70 (Mu et al., 2018), AURAMS (Galarnau et al., 2014), and CanMETO (Zhang et al., 2011a; Zhang et al.,
71 2011b; Zhang et al., 2009)). Efsthathiou et al. (2016) showed that considering absorption and adsorption
72 processes can better capture the concentration levels and seasonal variations of BaP. In recent years, the
73 effect of the heterogeneous reaction process of PAHs on transportation has also been studied. Mu et al.
74 (2018) developed a new kinetic scheme describing the effects of temperature and humidity on the organic
75 aerosol coating of BaP and BaP reaction rate. They found that low temperature and low humidity can
76 significantly increase the lifetime of BaP and enhance its LRT capacity.

77 However, the resolutions and spatial range differed greatly between these models. Most of the
78 models are either global or regional. There is a lack of simulation studies focusing on both global and
79 key regions, making it difficult to investigate a specific focus in a global background in a consistent
80 manner. Additionally, the resolution of most global models is low, which will further affect the health
81 risk assessment of PAHs. Furthermore, the up-to-date mechanisms (gas-particle partitioning,
82 heterogeneous reaction, and air-soil exchange) established for PAHs simulations are not considered in
83 earlier modeling studies.

84 China is one of the largest PAH-emitting countries in the world (Inomata et al., 2012; Zhang and
85 Tao, 2009). High concentrations of BaP have been reported (Bieser et al., 2012; Liu et al., 2014;
86 Shrivastava et al., 2017; Su et al., 2023). Over the polluted regions in eastern China, annual
87 concentrations of BaP exceeded 1 ng m^{-3} , the target values proposed in the European Union (EU) and
88 China. To improve air quality and protect public health, the State Council of China promulgated “the



89 Action Plan on Air Pollution Prevention and Control” (the Action Plan) in 2013. Since then, many studies
90 have investigated the changes in concentration levels and health risks of conventional pollutants, such as
91 PM_{2.5} (Feng et al., 2019; Wang et al., 2018; Zhang et al., 2019; Zhu et al., 2021; Wang et al., 2019). Wang
92 et al. (2019) pointed out that the annual average concentrations of PM_{2.5} in the Beijing-Tianjin-Hebei
93 (BTH), the Yangtze River Delta (YRD), and the Pearl River Delta (PRD) all decreased by more than 27%
94 in 2017, indicating that the control measures have achieved remarkable effects and the air quality has
95 been significantly improved. However, for non-conventional pollutants, such as BaP and other PAHs,
96 their concentration changes due to emission reduction in China after implementing of policies have not
97 been quantified. The changes in health risks and the benefits from control measures were not yet assessed.

98 Considering the aforementioned, we simulated PAHs from global to regional scales by coupling the
99 key physical and chemical modules associated with PAHs in a global-regional nested atmospheric
100 transport model. In particular, newly established parametrizations of gas-particle partitioning and
101 heterogeneous reaction were incorporated into the model. Then the changes in global concentration and
102 health risks of BaP over China were quantified based on model evaluation against a collected observation
103 dataset. The study can advance our understanding of global PAHs distribution and regional health risks
104 and their responses to emission change. The paper is arranged as follows: Section 2 briefly describes the
105 host model (IAP-AACM), the physical and chemical modules related to PAHs, and the method of
106 assessing health risks. Section 3 presents the configuration of the model and the observations used in the
107 evaluation. Section 4 shows the global and regional distributions of BaP concentrations and analyzes the
108 health risks associated with BaP in China. Section 5 discusses the uncertainty of the model. In Sect. 6,
109 the main conclusions are summarized.

110 **2 Model description and development**

111 **2.1 Description of host model**

112 The model used in this study is the Atmospheric Aerosol and Chemistry Model developed by the
113 Institute of Atmospheric Physics, Chinese Academy of Sciences (IAP-AACM) (Wei et al., 2019), which
114 was developed based on the Global Nested Air Quality Prediction Modeling System (GNAQPMS, Chen
115 et al., 2015; Wang et al., 2001). IAP-AACM is a 3-D Eulerian transport model that uses a multi-scale
116 domain-nesting approach to simulate atmospheric chemistry and aerosol processes from global to



117 regional scales. As recently described by Chen et al. (2015), compared with the traditional multi-scale
118 modeling methods (Seigneur et al., 2001), the online nesting method uses the same parameters in the
119 global and regional domains, which avoids uncertainties caused by different boundary conditions, and it
120 also provides boundary conditions at higher time resolution (Zhang et al., 2012b; Chen et al., 2015), thus
121 improving the performance of the model at the regional scale.

122 This model includes emission, horizontal and vertical advection (Walcek and Aleksic, 1998),
123 diffusion (Byun and Dennis, 1995), dry deposition (Zhang et al., 2003), gaseous chemistry (CBM-Z,
124 Carbon Bond Mechanism version Z, Zaveri and Peters, 1999), heterogeneous chemistry (Li et al., 2012),
125 aqueous reactions in clouds, and wet scavenging (Stockwell et al., 1990). It has been successfully and
126 widely applied to simulate the spatial-temporal distribution characteristics of gaseous pollutants, aerosol
127 components, and the long-distance transportation of mercury (Chen et al., 2015; Chen et al., 2014; Wei
128 et al., 2019; Ye et al., 2021; Du et al., 2019). In addition, advanced particle microphysics (APM) has been
129 incorporated to simulate new particle formation processes and predict the particle number concentrations
130 at global and regional scales (Chen et al., 2021).

131 **2.2 Development of the PAH module**

132 The PAH processes in the IAP-AACM model include gaseous-phase reaction, heterogeneous
133 reaction, gas-particle partitioning, air-soil exchange, dry deposition, and wet scavenging. The simulated
134 species include BaP, Benzo[b]fluorathene (BbF), Benzo[k]fluorathene (BkF), and Indeno[1,2,3-
135 cd]pyrene (IcdP) in the gas and particulate phases (Wu et al., 2024). In this study, we mainly focus on
136 BaP due to its highly carcinogenic nature and the relatively rich observations.

137 **2.2.1 Gaseous-phase reactions**

138 PAHs are degraded through reactions with various atmospheric oxidants such as hydroxyl radical
139 (OH), nitrate radical (NO₃), and ozone (O₃) in the troposphere (Lammel and Sehili, 2007). Among these
140 oxidants, the reactions with OH are considered to be the most important pathway for the removal of
141 PAHs. The nighttime reaction of PAHs with NO₃ is also important in the atmosphere (Keyte et al., 2013).
142 Therefore, reactions of gaseous-phase BaP with OH, NO₃, and O₃ are all considered in the model. The
143 second-order rate coefficients are 5.0×10^{-11} , 5.4×10^{-11} , and 2.6×10^{-17} cm³ molecules⁻¹ s⁻¹, respectively
144 (Inomata et al., 2013; Finlayson-Pitts and Pitts, 2000; Klöpffer et al., 2007).



145 2.2.2 Heterogeneous reaction

146 In the case of BaP, the heterogeneous reaction with O₃ is considered to be the dominant loss
147 (Finlayson - Pitts and Pitts, 2000; Efstathiou et al., 2016). Studies have shown that the process of
148 heterogeneous reaction can be well described by the Langmuir-Hinshelwood mechanism (Kahan et al.,
149 2006; Kwamena et al., 2007), in which BaP is adsorbed to the surface while the O₃ is in phase equilibrium.
150 The first-order reaction rate coefficient k (s⁻¹) of the Langmuir-Hinshelwood mechanism is as follows:

$$k = \frac{k_{max}K_{O_3}[O_3]}{1 + K_{O_3}[O_3]} \quad (1)$$

$$\frac{\partial C}{\partial t} = -K_{O_3}[O_3] \quad (2)$$

151 Where k_{max} is the maximum rate coefficient, and the value is 0.060±0.018 s⁻¹. [O₃] is the
152 concentration of O₃ (mol cm⁻³). K_{O_3} is the O₃ to surface equilibrium constant (0.028±0.014×10⁻¹³ cm³).

153 In addition, we incorporated a more detailed parameterization (ROI-T) developed by Mu et al. (2018)
154 based on the Langmuir-Hinshelwood mechanism. The scheme emphasizes the importance of
155 representing the dependence of degradation on temperature and humidity, when coated by organic
156 aerosols. The first-order reaction rate coefficient k (s⁻¹) is given by Eq. (3).

$$k = base + \frac{max - base}{1 + (\frac{xhalf}{[O_3]})^{rate}} \quad (3)$$

157 Where $base$, max , $rate$, and $xhalf$ are all the parameterizations of the heterogeneous reaction,
158 with specific values shown in Mu et al. (2018). In our study, we coupled these two parameterizations as
159 two options for O₃ degradation by heterogeneous reaction in IAP-AACM. The model results using these
160 two schemes were compared to analyze the influence of heterogeneous reaction schemes on BaP
161 concentration. The ROI-T scheme was used as the default in this study.

162 2.2.3 Gas-particle partitioning

163 The partition of compounds between the gas and particulate phases is parameterized with the gas-
164 particle partitioning coefficient (K_p , m³ μg⁻¹) (Harner and Bidleman, 1998):

$$K_p = \frac{[PAH]_p}{[TSP]} / [PAH]_g \quad (4)$$

165 Where [PAH]_g and [PAH]_p are the concentrations of PAHs in the gas and particulate phase
166 (μg m⁻³), and [TSP] is the concentration of total suspended particles (TSP, μg m⁻³) in the atmosphere



167 ($\mu\text{g m}^{-3}$).

168 Adsorption onto black carbon (BC) and absorption into aerosol organic matter (OM) are two
 169 important mechanisms of gas-particle partitioning (Odabasi et al., 2006). Therefore, we use the gas-
 170 particle partition coefficient equation to represent these two mechanisms, which was derived by Dachs
 171 and Eisenreich, 2000:

$$K_p = \frac{(f_{OM} MW_{OCT} \delta_{OCT}) K_{OA}}{(\rho_{OCT} MW_{OM} \delta_{OM} 10^{12})} + \left[\left(\frac{f_{BC} a_{BC} K_{SA}}{a_{AC} 10^{12}} \right) \right] \quad (5)$$

172 Where MW_{OCT} and MW_{OM} are the mean molecular weights of octanol and OM phase (g mol^{-1}),
 173 δ_{OCT} and δ_{OM} are the activity coefficient of the absorbing compound in octanol and OM phase,
 174 respectively. f_{OM} and f_{BC} are the mass fractions of OM phase on TSP and the BC in the aerosol. ρ_{OCT}
 175 is the density of octanol (0.820 kg L^{-1}). a_{BC} and a_{AC} are the specific surface areas of BC ($62.7 \text{ m}^2 \text{ g}^{-1}$,
 176 Jonker and Koelmans, 2002) and activated carbon (AC), respectively. In this study, we use the same
 177 assumption as Odabasi et al. (2006) ($MW_{OCT}/MW_{OM} = 1$, $\delta_{OCT}/\delta_{OM} = 1$, and $a_{BC}/a_{AC} = 1$).

$$\log K_{OA} = A + B/(T) \quad (6)$$

178 Where K_{OA} is the octanol–air partitioning coefficient (temperature dependent). T is the
 179 temperature (K). The values of A and B are 5382 and -6.5, respectively (Odabasi et al., 2006).

$$\log P_L = m_L(T)^{-1} + b_L \quad (7)$$

$$\log K_{SA} = -0.85 \log P_L + 8.94 - \log \left(\frac{998}{a_{BC}} \right) \quad (8)$$

180 Where P_L is the supercooled liquid vapor pressure (Pa). The values of b_L and m_L are 12.59 and
 181 -5252, respectively (Dachs and Eisenreich, 2000). K_{SA} is the soot–air partitioning coefficient (L kg^{-1}),
 182 which is a function of P_L and a_{BC} (van Noort, 2003).

183 2.2.4 Air-soil exchange

184 The semi-volatility and persistence of PAHs allow them to dynamically exchange between the
 185 atmosphere and soil by deposition and re-volatilization from ground surfaces (Semeena and Lammel,
 186 2005). These processes can affect the distribution and long-distance transport of PAHs in the environment.
 187 As described by Hansen et al. (2004), air–soil exchange is parameterized following Strand and Hov
 188 (1996), which is based on Jury et al. (1983). Here, soil (standard soil) is considered to be a homogeneous
 189 layer of thickness $z_s = 0.15 \text{ m}$, and standard values and chemical properties are provided by Jury et al.
 190 (1983) (Table S1). The differential equation for the change of concentrations in soil and air can be



191 expressed by Eq. (9) and Eq. (10):

$$\frac{\partial c_s}{\partial t} = \frac{1}{z_s} (F_{exc,soil} + F_{wet}) - k_{soil} c_s \quad (9)$$

$$\frac{\partial c_a}{\partial t} = -\frac{1}{z_a} F_{exc,soil} \quad (10)$$

192 Where C_a and C_s are the concentrations of PAHs in the atmosphere and soil, respectively. The z_a
 193 is the lowest atmospheric layer depths (m), F_{wet} is the wet deposition flux ($\text{mol s}^{-1} \text{m}^{-2}$). k_{soil} is the
 194 degradation rate in soil, which is estimated to be $2.2 \times 10^{-8} \text{ s}^{-1}$ (Finlayson - Pitts and Pitts, 2000; Klöpffer
 195 et al., 2007; Lammel et al., 2009). The air–soil exchange flux ($F_{exc,soil}$) is given by Eq. (11):

$$F_{exc,soil} = K_{a/s} \left(c_a - \frac{c_s}{K_{soil-air}} \right) \quad (11)$$

196 $K_{soil-air}$ is the partitioning coefficient between soil and air, which is given by Karickhoff (1981):

$$K_{soil-air} = 4.11 \times 10^{-4} \times \rho_s f_{OC} K_{OA} \quad (12)$$

197 Where f_{OC} is the fraction of OC in soil and 4.11×10^{-4} is a constant with units of $\text{m}^3 \text{kg}^{-1}$. ρ_s is the
 198 density of soil. $K_{a/s}$ is the overall exchange velocity (m s^{-1}), which can be estimated by Eq. (13) (Strand
 199 and Hov, 1996):

$$K_{a/s} = \frac{D_G^{air} a^{10/3} (1-l-a)^{-2} + D_L^{water} l^{10/3} K_{WA} (1-l-a)^{-2}}{z_s/2} \quad (13)$$

200 Where D_G^{air} and D_L^{water} are the air and liquid diffusion coefficient ($\text{m}^2 \text{s}^{-1}$), respectively. K_{WA} is
 201 the water-air partitioning coefficient. The differential equation is solved the ODEPACK
 202 (<https://github.com/jacobwilliams/odepack>).

203 2.2.5 Dry and wet deposition

204 PAHs can be removed from the atmosphere and enter terrestrial ecosystems through dry and wet
 205 deposition (Cao et al., 2021). Dry deposition and wet scavenging have been included in IAP-AACM. For
 206 the gaseous species of PAHs, their wet scavenging is assumed to be the same as xylene in the CBMZ
 207 mechanism, which is also an aromatic hydrocarbon like BaP; for the PAHs in the particle phase, these
 208 two processes are treated similarly to that of organic aerosol.

209 2.3 Risk assessment

210 The incremental lifetime cancer risk (ILCR) is widely used to calculate the risk of human exposure
 211 to PAHs (Nam et al., 2021). The carcinogenic risk of PAHs to humans through different exposure routes



212 was calculated based on the health risk evaluation model proposed by the U.S. Environmental Protection
213 Agency (EPA) (Smith et al., 1999).

214 The national population data in 2013 and 2018 were obtained from the LandScan (Oak Ridge
215 National Laboratory; database can be accessed via: <https://landscan.ornl.gov>, last access: 20 January
216 2024) and re-gridded to $1^{\circ} \times 1^{\circ}$ and $0.33^{\circ} \times 0.33^{\circ}$ to match the model resolution.

217 2.3.1 Daily exposure dose

218 Dermal contact and inhalation are regarded as the major routes of human exposure to BaP (Li et al.,
219 2010; Ma et al., 2020; Zhang et al., 2016). In this study, the health risk for the entire population and three
220 groups (adult women, adult men, and children) are calculated. The daily exposure dose (ADD) to PAHs
221 through the two exposure routes is calculated as follows:

$$222 \quad ADD_{der} = \frac{C \times SA \times ABS \times AF \times EF \times ED \times CF}{AT \times BW} \quad (14)$$

$$223 \quad ADD_{inh} = \frac{C \times IR \times EF \times ED}{AT \times BW} \quad (15)$$

224 Where ADD_{der} and ADD_{inh} are the average daily exposure dose that enters the body through the
225 dermal contact and inhalation, respectively ($\text{ng kg}^{-1} \text{ day}^{-1}$), C is the concentration of PAHs (ng m^{-3}). IR
226 is the inhalation rate ($\text{m}^3 \text{ d}^{-1}$). EF and ED are the exposure duration (d a^{-1}) and period (a), respectively.
227 BW is the body weight (kg). SA is the skin exposed surface area (cm^2). ABS is the skin absorption
228 factor. AT is the average exposure time (d). The values are shown in Table S2.

229 2.3.2. Incremental lifetime cancer risk (ILCR)

230 The ILCR was calculated based on the ADD:

$$231 \quad ILCR_{der} = ADD_{der} \times SFO_{der} / 10^6 \quad (16)$$

$$232 \quad ILCR_{inh} = ADD_{inh} \times SFO_{inh} / 10^6 \quad (17)$$

$$233 \quad TILCR = ILCR_{der} + ILCR_{inh} \quad (18)$$

234 Where $ILCR_{der}$ and $ILCR_{inh}$ are lifetime cancer risks through the dermal contact and inhalation,
235 respectively. $TILCR$ is the total lifetime cancer risk of exposure through the two pathways. SFO is a
236 cancer slope factor (kg day mg^{-1}), and its values are shown in Table S2. For carcinogen, an $ILCR$ less
237 than 1×10^{-6} indicates negligible cancer risk, an $ILCR$ between 1×10^{-6} and 1×10^{-4} indicates potential
238 cancer risk, and an $ILCR$ larger than 1×10^{-4} indicates high potential cancer risk.

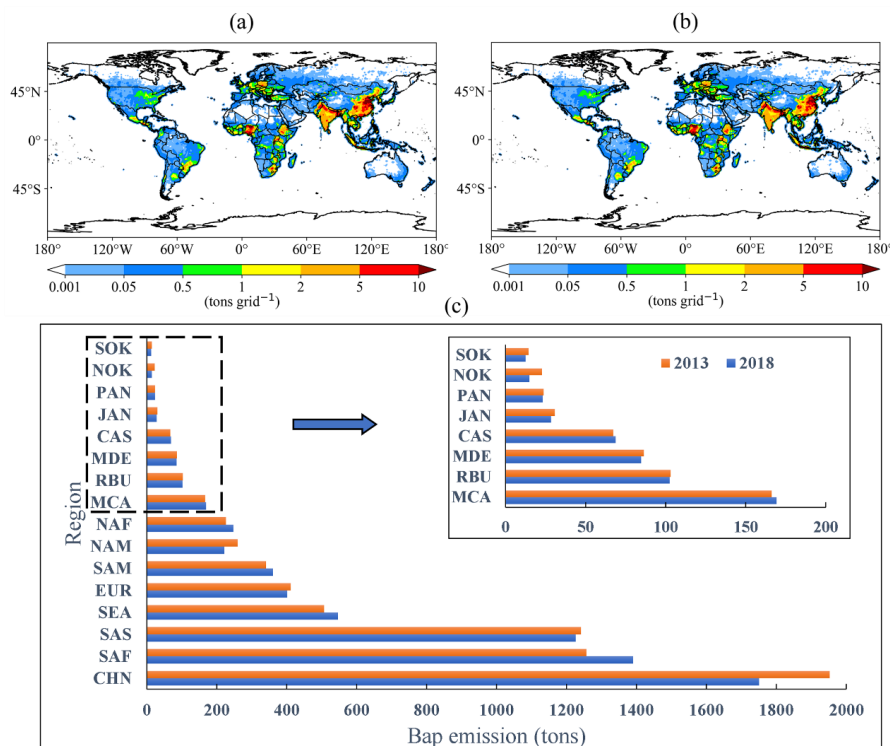


234 **3 Experiments setup and observation data**

235 **3.1 Experiments setup**

236 In this study, we used two nested domains covering the whole globe and East Asia as shown in Fig.
237 S1. The horizontal resolutions are $1^{\circ} \times 1^{\circ}$ and $0.33^{\circ} \times 0.33^{\circ}$, respectively. A total of 20 vertical layers are
238 used in IAP-AACM. The first layer of the model is approximately 50 m deep and the top layer extends
239 to 20 km. The simulation results from January 1st to December 31st 2013 and from January 1st to
240 December 31st 2018 were used for analysis. Each simulation had a one-month spin-up before January 1st
241 to reduce the influence of initial conditions. The global version of the Weather Research and Forecasting
242 model (WRF, version 3.7.1) (Zhang et al., 2012a; Skamarock et al., 2008) provides the meteorological
243 fields to drive the IAP-AACM. The initial and boundary conditions of the global WRF were produced
244 by Final Analysis data (FNL) from the National Centers for Environmental Prediction (NCEP).

245 The emission inventory of BaP in 2013 and 2018 was derived from the Emissions Database for
246 Global Atmospheric Research (EDGAR, Crippa et al., 2020, available from
247 https://edgar.jrc.ec.europa.eu/dataset_pop60#sources, last access: 15 December 2023). We mainly
248 analyzed the results using EDGAR emission, which mainly includes anthropogenic sources such as
249 power, transportation, industrial, agricultural, and energy for buildings. An additional simulation for 2013
250 using the emission inventory developed by the research group of Peking University (PKU)
251 (<http://inventory.pku.edu.cn>, last access: 10 February 2023) was used to investigate the uncertainties
252 from emissions. The resolution of both emission inventories is $0.1^{\circ} \times 0.1^{\circ}$. Therefore, we re-gridded the
253 emissions inventories to match the model grids at $1^{\circ} \times 1^{\circ}$ and $0.33^{\circ} \times 0.33^{\circ}$ resolution.



254

255

256

Figure 1. Spatial distributions of total emissions of BaP in 2013 (a) and 2018 (b) based on the EDGAR inventory. BaP emissions for 16 regions (except oceans, Arctic, and Antarctic) in 2013 and 2018 (c).

257

258

259

260

261

262

263

264

265

266

267

The global total emissions of BaP in 2013 and 2018 are shown in Fig. 1a and 1b, respectively. The annual emissions in different regions (Fig. S1) were also calculated (Fig. 1c). The global emissions of BaP were 7,166.9 in 2013 and 7,109.5 t in 2018, respectively. The global emission showed a slight decrease of (0.8%) from 2013 to 2018. China is one of the largest BaP-emitting countries in the world. Its emissions were 1,952.2 t in 2013 and 1,750.2 t in 2018, respectively, accounting for about 27.2% and 24.6% of the world. Southern Africa and India had the second and third-largest emissions. Emissions from China, Southern Africa, and India accounted for 62.1% and 61.4% of the world. China, Australia, India, Europe, North America, South Korea, Japan, and North Korea displayed a declining trend from 2013 to 2018. China experienced the largest decline (10.4%) due to the active emission control measures taken under the “Air Pollution Prevention and Control Action Plan” implemented in 2013. The emissions increased in Africa (10.7%), South-East Asia (7.8%), and South America (5.9%).



268 To understand the change in BaP concentrations, we conducted five experiments: the first and
269 second experiments simulated the BaP concentration using the emissions in 2013 and 2018 driven by the
270 corresponding meteorological fields. The third experiment used the emission in 2018 but kept the
271 meteorological conditions in 2013 to investigate the effects of meteorological condition changes on the
272 concentration of BaP. Studies neglecting the heterogeneous loss of BaP and using two different
273 heterogeneous schemes were also performed to explore the impacts of heterogeneous reactions on BaP
274 concentrations in the fourth and fifth experiments

275 **3.2 Observational data**

276 To evaluate the model performance, we collected the PAHs observation from several available
277 datasets and more than 50 published papers. The observational data are summarized as follows: (1)
278 European Monitoring and Evaluation Program (EMEP, available from
279 <https://projects.nilu.no/ccc/reports.html>, last access: 15 December 2023): this includes annual and
280 monthly averages of BaP concentrations at 36 European sites in Spain, Finland, France, Germany,
281 Norway, Poland, and other countries in Europe; (2) National Air Pollution Surveillance network: (NAPS,
282 <https://data-donnees.az.ec.gc.ca/data/air/monitor/>: last access: 30 January 2024): this includes daily
283 averages (autumn and winter) of BaP concentrations at Canadian stations; (3) Integrated Atmospheric
284 Deposition Network: (IADN, <https://iadnviz.iu.edu/datasets/index.html>, last access: 20 January 2023):
285 this includes monthly mean concentrations of BaP at 6 sites in the United States and Canada from 1990
286 to 2021; (4) Chinese Persistent Organic Pollutants (POPs) Soil and Air Monitoring Program Phase II
287 (SAMP-II, Ma et al., 2018): this is carried out by the International Joint Research Center for Persistent
288 Toxic Substances (IJRC-PTS), focusing on 11 urban centers in China (Beijing, Xi'an, Nanchang,
289 Kunming, Lanzhou, Chengdu, Harbin, Dalian, Lhasa, Guangzhou, and Shihezi), 1 suburb and 3
290 background/rural areas. This observational data only covers the period from August 2008 to July 2010;
291 (5) observational data collected from published papers (these sources are listed in supplementary material)
292 (Wu et al., 2024).

293 PAHs measurements data are very sparse compared to conventional pollutants (e.g., $PM_{2.5}$). Since
294 most of the data are not continuous in time, we selected data covering at least 10 days in years as close
295 as possible to the simulation year (2013) and used the mean values for comparison. The comparison of
296 the monthly variation was conducted only for sites in Europe where observations were continuous and

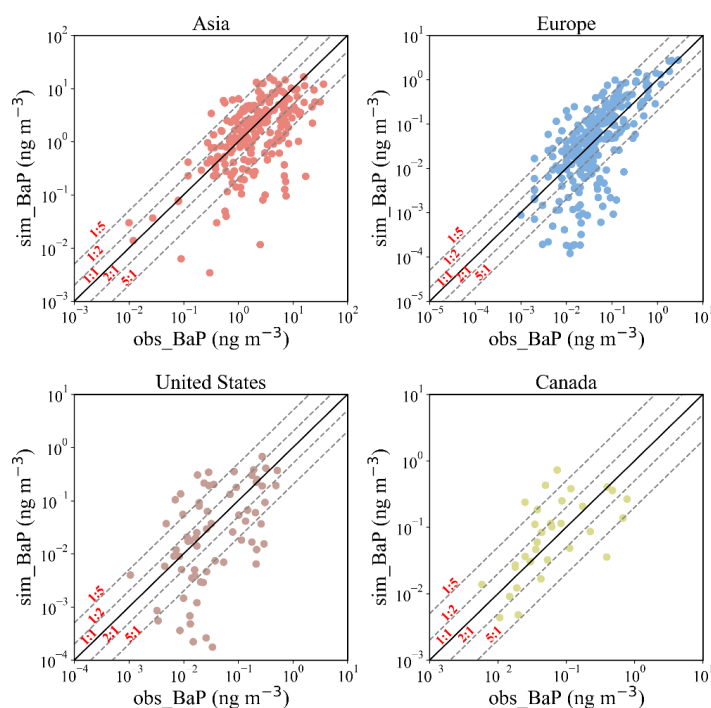


297 available. The locations of the BaP observation sites are shown in Fig. S2. The site information is listed

298 in Table S5 and Table S6.

299 4 Results

300 4.1 Global distribution of BaP

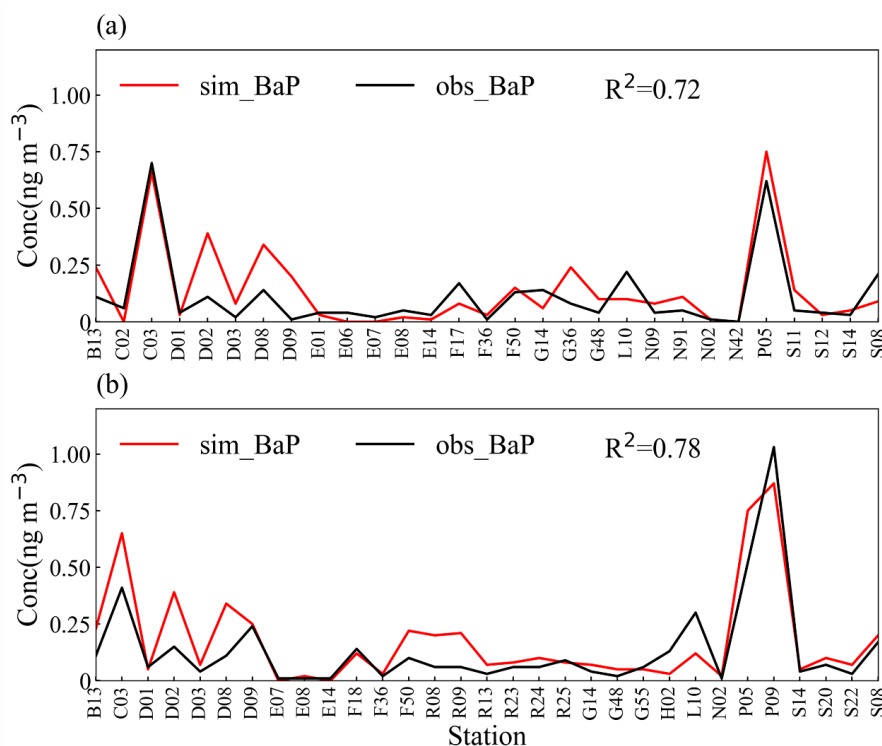


301

302 **Figure 2. Comparison of simulated (sim_BaP) and observed (obs_BaP) annual mean concentrations of BaP**

303 **in Asia (orange), Europe (blue), United States (brown), and Canada (green) in 2013. The solid black line**

304 **shows a ratio of 1 : 1 and the dashed gray lines show ratios of 5 : 1, 2 : 1, 1 : 2, and 1 : 5.**



305

306

307

Figure 3. Comparison of the BaP annual mean simulated (red) concentrations with observed (black) values at European sites in 2013 (a) and 2018 (b).

308

309

310

311

312

313

314

315

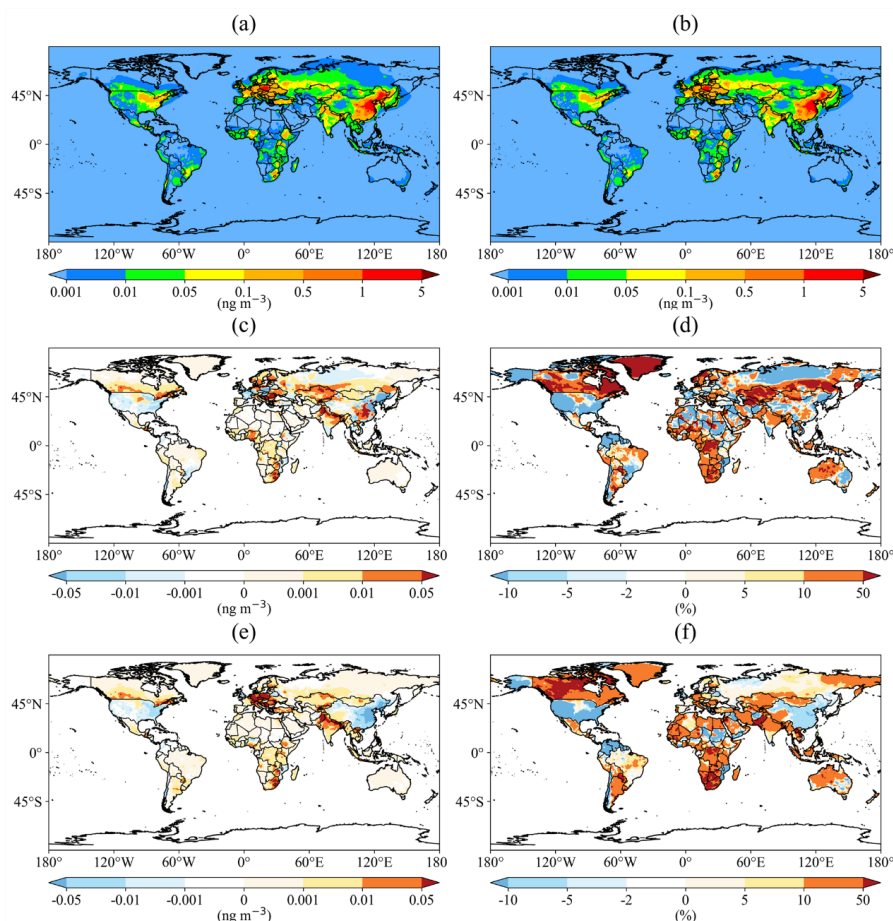
316

317

318

319

To evaluate the performance of the IAP-AACM model, annual mean simulated concentrations in Asia, Europe, the United States, and Canada were compared with observations (Fig. 2). The results show that the model can reproduce nearly half of the observation samples within a factor of 2 and most observations within a factor of 5 at sites in Asia, Europe, the United States, and Canada. The number of sites where BaP was underestimated was greater than the number where it was overestimated due to the averaging effect of subgrid emissions. Considering that some of the comparisons are not in the same year, a certain discrepancy between the model and observation is expected. Further, a specific comparison was performed using the data from about 30 stations in Europe (Fig. 3a and b). High concentrations were mainly found in polluted areas of Central Europe, consistent with the simulation of Gusev et al. (2017), such as Poland (P05) and the Czech Republic (C03) with observed values of 0.70 and 0.62 ng m⁻³, respectively, and simulated concentrations of 0.66 and 0.75 ng m⁻³ in 2013. The model successfully reproduced the observed concentrations and differences between sites.



320

321

322

323

Figure 4. Spatial distributions of annual mean BaP concentrations based on the EDGAR in 2013 (a) and 2018 (b). The absolute (c/e) and relative concentration changes (d/f) from 2013 to 2018 are shown considering both emissions and meteorological conditions (c, d) or only emissions (e,f), respectively.

324

325

326

327

328

329

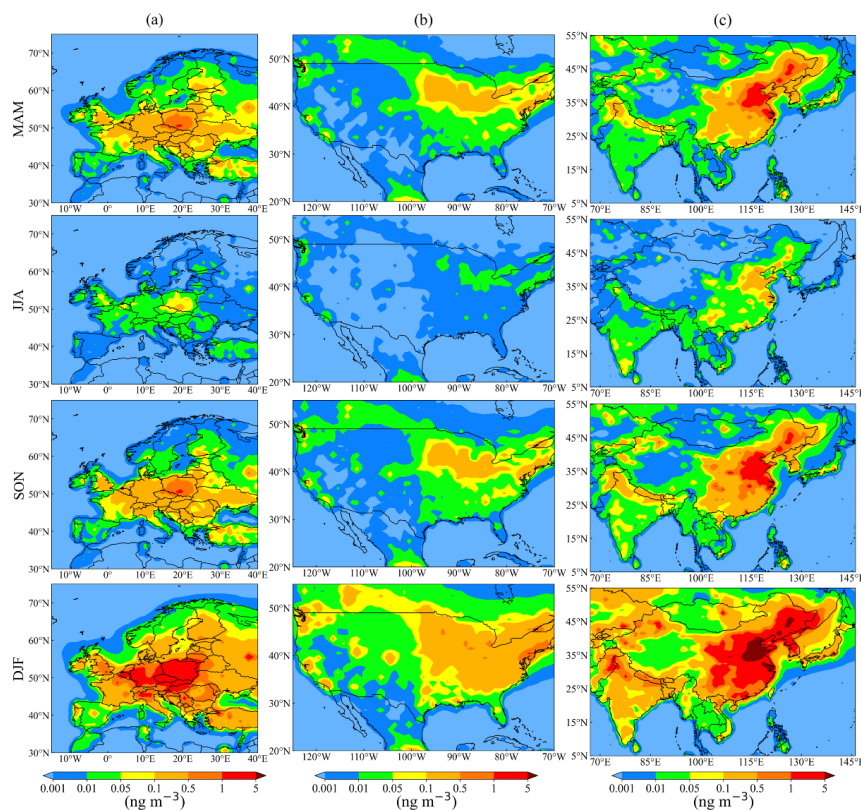
330

331

The spatial distribution of annual mean BaP concentrations based on the EDGAR inventory in 2013 and 2018 are shown in Fig. 4a and b. The spatial distribution of BaP concentrations in 2018 was similar to that in 2013. The spatial pattern was consistent with the emission distribution in the EDGAR inventory. High concentrations of BaP were found in northern and eastern China, and central Europe, even exceeding the European Union target value for BaP (1 ng m^{-3}), indicating an urgent need to control BaP and other PAHs. The absolute and relative concentration changes from 2013 to 2018 are shown in Fig. 4c and d. The most significant decreases were seen in Russia, the United States, eastern and northern China. By contrast, the concentration in India, Europe, Southeast Asia, and South Africa shows an



332 increase, with the average annual concentration increasing by 19.4%, 1.2%, 11.2%, and 18.3%,
333 respectively. When only considering the impact of emission change (Fig. 4e and f), the decrease in the
334 eastern United States is larger and the increase in central Europe is larger. In particular, there is an obvious
335 decline (about 8.0%) across China, which demonstrates the effect of the emission reduction measures.
336 These results clearly show the large influence of meteorological changes. It is crucial to consider
337 meteorological factors when evaluating emission changes and reduction measures through monitoring
338 concentrations in the atmosphere.

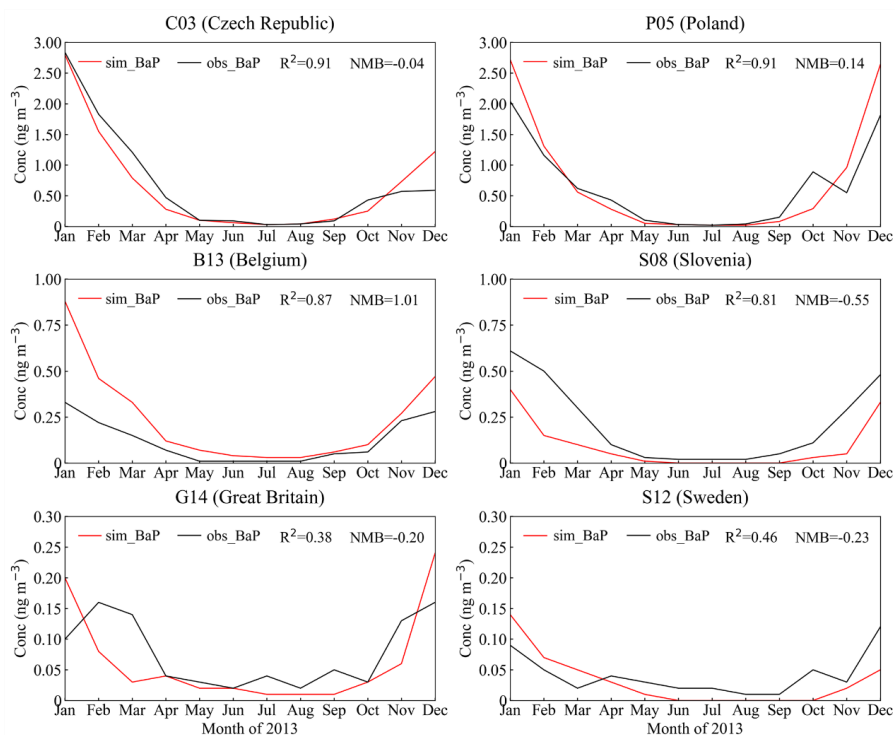


339
 340 **Figure 5. Spatial distributions of seasonal mean concentrations in Europe (a), the contiguous United States**
 341 **(b), and East Asia (c) in 2013.**

342 Figure 5 shows the seasonal mean concentrations of BaP in Europe, the contiguous United States,
 343 and East Asia in four seasons: March–April–May (MAM, representing spring), June–July–August (JJA,
 344 representing summer), September–October–November (SON, representing autumn), and December–
 345 January–February (DJF, representing winter). Generally, BaP had the highest concentration in winter and
 346 lowest in summer. This is caused by the larger emission and poorer atmospheric diffusion conditions in
 347 winter than in summer. In the contiguous United States, the concentrations were lower than 1 ng m^{-3} in
 348 all four seasons, consistent with the simulation of Galarneau et al. (2014). In east China, large areas have
 349 a concentration of $> 1 \text{ ng m}^{-3}$ and even $> 5 \text{ ng m}^{-3}$ in BTH in winter. Europe shows a distribution of high
 350 values in central areas and low values in remote areas. In Central Europe (such as Poland and the Czech
 351 Republic), large areas have concentrations between $1\text{--}5 \text{ ng m}^{-3}$ in winter. High concentrations were also
 352 reported by Bieser et al. (2012). The observation clearly shows higher concentrations at sites in Poland
 353 and the Czech Republic than at other sites in Europe (Fig. 6). The model successfully reproduces the



354 seasonal variation of BaP at sites in Europe. The simulation had a good agreement with observations at
 355 C03 and P05 with correlation coefficient (R^2) of 0.91 and 0.91, and normalized mean bias (NMB) of -
 356 0.04 and 0.14, respectively. The R^2 was higher than 0.8 at B13 and S08, and the NMB was 1.01 and -
 357 0.55. In summary, IAP-AACM can reasonably simulate the spatial distribution and seasonal variation of
 358 BaP.



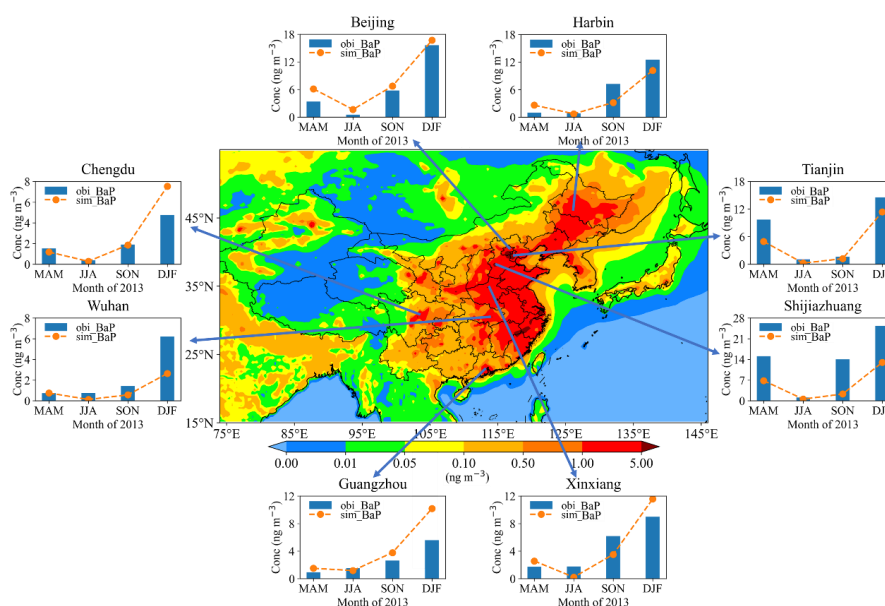
359
 360 **Figure 6. Comparison of the BaP month mean simulated concentrations (red) with observed values (black)**
 361 **at six stations in Europe in 2013.**

362 4.2 Distribution of PAHs and their change in China

363 Figure 7 shows the annual mean distribution of BaP in China in 2013. The concentrations ranged
 364 from 0.02 to 6.14 ng m^{-3} . Overall, high concentrations were simulated in the North China Plain, East
 365 China, and Northeast China, significantly higher than in Northwest and Southwest China, consistent with
 366 previous studies (Ma et al., 2020; Yan et al., 2019). Among the different provinces in China, there are 14
 367 provinces with concentrations higher than the ambient air quality standards of China (1 ng m^{-3} , GB 3095–
 368 2012: <http://www.zhb.gov.cn/>, last access: 6 April 2014). Shanghai had the highest concentration of 6.14
 369 ng m^{-3} , followed by Tianjin (4.56 ng m^{-3}), Beijing (3.41 ng m^{-3}), and Shandong (3.10 ng m^{-3}). The



370 concentrations in the Northwest and Southwest regions were lower, with Tibet having the lowest
 371 concentration of only 0.02 ng m⁻³. This is due to lower levels of industrial activities and population
 372 density in these regions compared to eastern regions. In addition, the high topography of northwest
 373 regions has good air circulation and is conducive to the diffusion and dilution of atmospheric pollutants.
 374 In 2013, Beijing had the highest BaP concentration in winter (14.03 ng m⁻³), possibly due to the high
 375 population density, high number of vehicles, and frequent industrial activities in Beijing. Moreover,
 376 Beijing lies on the North China Plain, where the meteorological conditions make it easier for air
 377 pollutants to stay and accumulate, resulting in a high concentration of BaP.



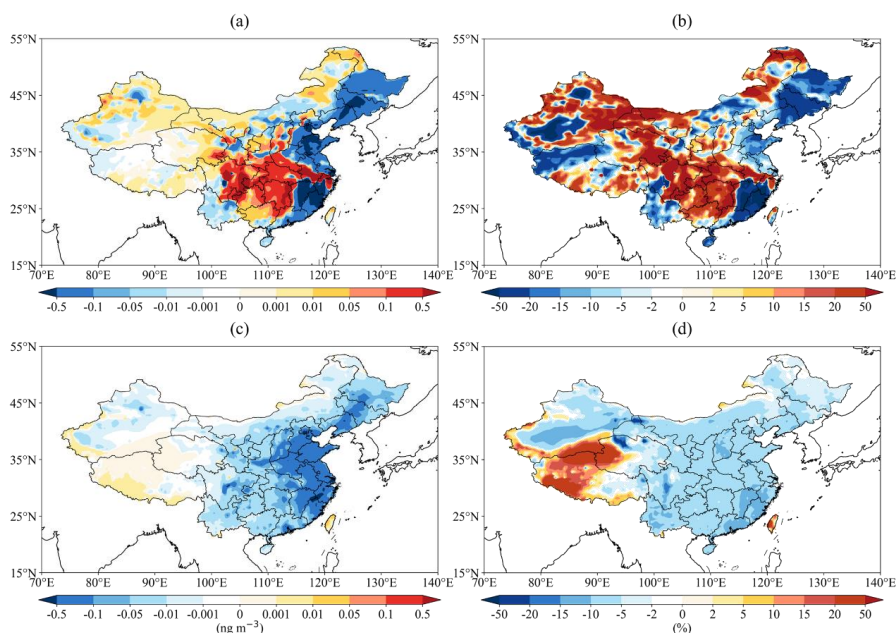
378
 379 **Figure 7. Spatial distributions of annual mean concentrations in China. Comparison of the BaP month mean**
 380 **simulated concentrations (red) with observed values (black) at eight cities in 2013.**

381 To reveal the seasonal variation of BaP concentrations in key regions, we analyzed the concentration
 382 in eight major cities, i.e., Beijing, Tianjin, Shijiazhuang, Xixiang, Wuhan, Chengdu, Guangzhou, and
 383 Harbin (seen in Fig. 7). It can be seen that the seasonal variations of BaP in these cities are similar, with
 384 the highest values in winter and the lowest in summer. The seasonal difference in northern cities was
 385 significantly greater than that in southern cities. In Beijing, Xixiang, Tianjin, Harbin, and Shijiazhuang,
 386 the differences in concentration between winter and summer were as high as 15.06, 11.76, 11.14, 9.45,
 387 and 12.42 ng m⁻³, respectively. This is caused by the fact that coal-fired heating is very common in
 388 northern China, which can significantly increase the PAH emissions in winter (Yan et al., 2019). In



389 addition, the meteorological conditions also affect the seasonal variation of PAHs, as the lower
390 temperature, less rainfall, and weaker solar radiation during the winter support the formation of a stable
391 inversion layer, greatly limiting the diffusion of BaP in the air (Lin et al., 2015; Quan et al., 2014).

392 By comparing the simulated concentrations with the observed concentrations, we find that the model
393 can capture the BaP concentrations and the seasonal pattern in different cities. For example, the observed
394 and simulated concentrations show good consistency in the spring, summer, and autumn of Chengdu and
395 in the summer, autumn, and winter of Beijing, with a deviation of only 0.04 to 1.1 ng m⁻³. However, there
396 were some deviations between the simulated and observed concentrations. The most obvious
397 underestimation is seen in Shijiazhuang. This is probably due to the underestimation of emissions and
398 the model resolution that may not fully resolve the pollution in cities with urban areas smaller than the
399 model grid. The model performance could be improved by using more precise emissions and increasing
400 grid resolution. Nonetheless, the model can capture the magnitude and seasonal variation in BaP
401 concentration well in China and in other countries around the world, and can therefore be used to evaluate
402 the health effects of BaP exposure.

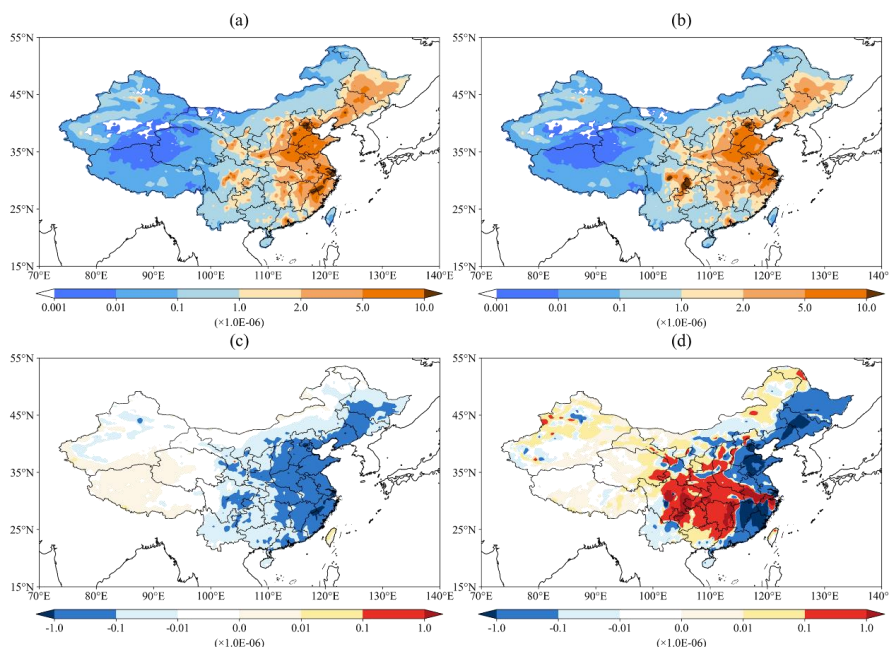


403
404 **Figure 8. The absolute (a/c) and relative concentration changes (b/d) from 2013 to 2018 in mean annual BaP**
405 **concentrations in China are shown considering both emissions and meteorological conditions (a, b) or only**
406 **emissions (c, d), respectively.**



407 The changes from 2013 to 2018 are shown in Fig. 8. The trend and magnitude of changes differ
408 greatly across different regions. The largest decrease (> 20%) was seen in northeastern and southeastern
409 China. The concentration also decreased in the North China Plain. The decrease was larger than the
410 emission reduction over these areas. By contrast, as shown in Fig. 8a, the concentration in the Sichuan
411 Basin showed an inverse trend although the emission decreased. This phenomenon reflects the impact of
412 meteorological conditions. When only considering the emissions changes, the concentration shows a
413 decrease over most regions consistent with the emission change. It should be noted that the decrease in
414 BaP in the two experiments is significantly lower than that of PM_{2.5}. Wang et al. (2019) showed that
415 compared with 2013, the concentration of PM_{2.5} in the BTH, the YRD, and the PRD in 2017 decreased
416 by 39.6%, 34.3%, and 27.7%, respectively. For cities in North and East China, the concentration still
417 exceeds the national limit value (1 ng m⁻³) although the concentration of BaP decreased significantly in
418 2018. For example, the BaP concentrations in Shanghai, Beijing, and Tianjin considering changes in both
419 emissions and meteorology were 5.32, 3.31, and 3.38 ng m⁻³, respectively, and those with emission
420 changes alone were 5.58, 3.11, and 4.17 ng m⁻³, indicating that the concentrations are mainly affected by
421 the emission sources. The results in the central and western cities differed greatly between the two
422 experiments, especially in Chongqing, Sichuan, and Guizhou, indicating that changes were mainly
423 related to meteorological conditions. Therefore, when formulating emission reduction policies, it is
424 necessary to take into account the effects of changes in meteorological conditions as well as emission
425 sources.

426 **4.3 Health risks of PAHs in China**



427

428 **Figure 9. The distribution of TILCR (the sum of ILCR values of the two exposure routes) in China in 2013**
 429 **(a) and 2018 (b), and the absolute from 2013 to 2018 when only emissions (c) or both emissions and**
 430 **meteorological conditions (d) are considered.**

431

432

433

434

435

436

437

438

439

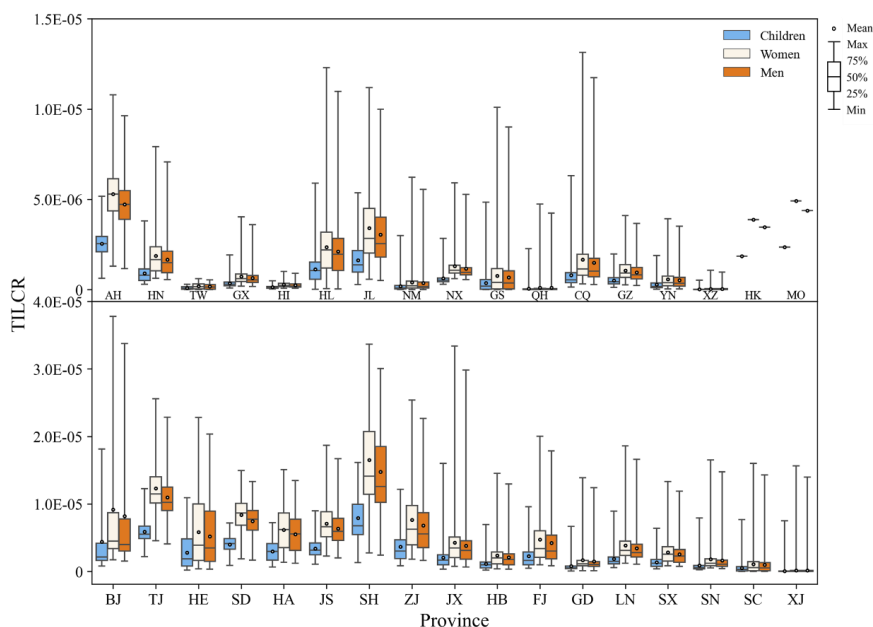
440

441

442

443

In this section, the health risks of BaP are assessed based on the simulation over the nested domain (domain 2) covering China. The ILCR induced by inhalation and dermal contact to BaP based on exposure for children, adult women, and adult men were calculated using Eq. (14)–Eq. (18). Figure. 9a and b show the distribution of TILCR (the sum of ILCR values of the two exposure routes) in China in 2013 and 2018, and Fig. 9c and d show the change from 2013 to 2018 when only emissions or both emissions and meteorological conditions are considered. It can be seen that the spatial distribution of TILCR (Fig. 9a) is consistent with the spatial distribution of the BaP annual concentrations (Fig. 7), showing higher risk in eastern regions than in the western regions (Han et al., 2020). The values of the TILCR in China ranged from 1.6×10^{-9} to 3.8×10^{-5} , with an average value of 3.7×10^{-7} . Compared with 2013, the average TILCR in 2018 decreased by 3.0×10^{-8} , which is mainly directly related to the decrease in concentration. From the perspective of two exposure routes, $ILCR_{inh}$ and $ILCR_{der}$ values ranged from 1.5×10^{-10} – 3.9×10^{-6} and 1.4×10^{-9} – 3.4×10^{-5} , with an average value of 3.9×10^{-8} and 3.3×10^{-7} , respectively. The values of $ILCR_{der}$ were one order of magnitude higher than the $ILCR_{inh}$.



444

445

446

Figure 10. The TILCR values for the three age groups (Children, Women, and Men) in different provinces of China in 2013.

447

448

449

450

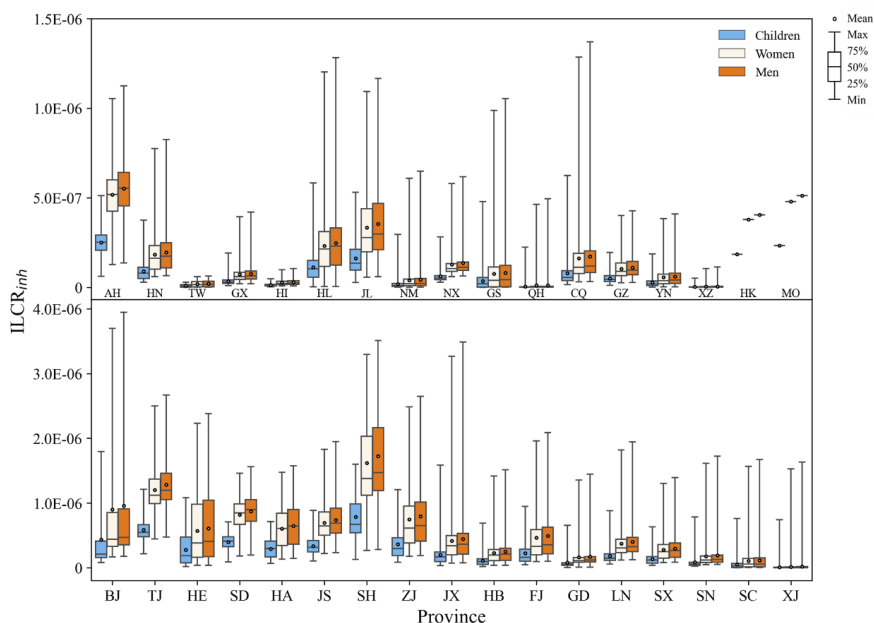
451

452

453

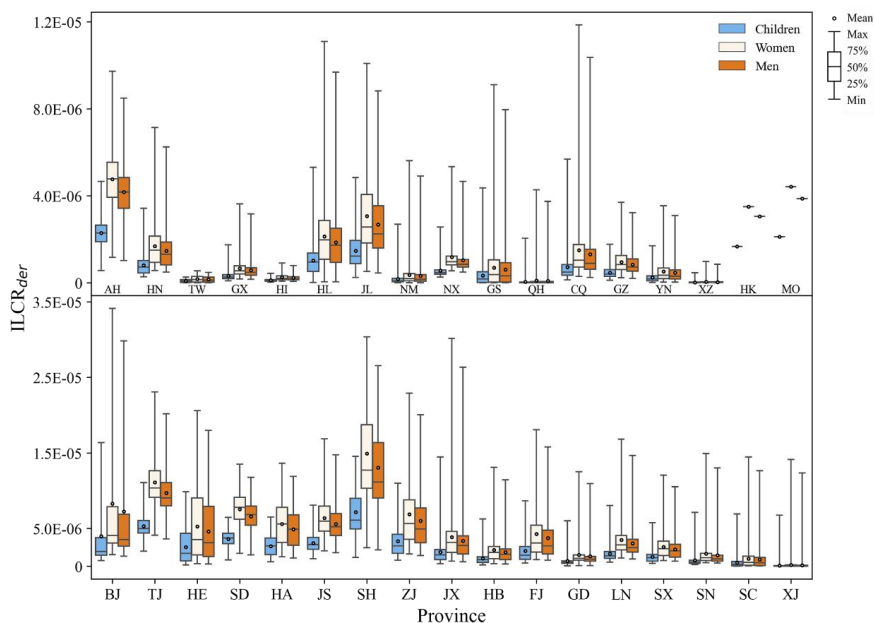
454

The TILCR values of the three groups in 2013 and 2018 are shown in Fig. 10 and Fig. S3 (the provinces are listed in Table S4), respectively, which ranged from 1.55×10^{-9} to 3.78×10^{-5} (1.60×10^{-9} to 3.41×10^{-5}). The order of TILCR was women (1.46×10^{-6}) > men (1.31×10^{-6}) > children (7.03×10^{-7}), which was similar to that of dermal contact exposure. Overall, 29.2% of TILCR were higher than 1.0×10^{-6} , and 1.2% of TILCR were higher than 1.0×10^{-5} in 2013. There was a slight decrease in TILCR values in 2018 due to the lower concentrations of BaP, with 27.9% and 0.7% of TILCR higher than 1.0×10^{-6} and 1.0×10^{-5} , respectively. There is no high cancer risk in China, but there are potential cancer risks in some areas, which should be paid attention to.



455
456
457

Figure 11. The $ILCR_{inh}$ values for the three age groups (Children, Women, and Men) in different provinces of China in 2013.



458
459
460

Figure 12. The $ILCR_{der}$ values for the three age groups (Children, Women, and Men) in different provinces of China in 2013.

461 The $ILCR$ values of the three groups in China through inhalation and dermal exposure routes are



462 shown in Fig. 11 and Fig. 12, and the ILCR in 2018 are shown in Fig. S4 and Fig. S5. For the inhalation
463 pathway, the average $ILCR_{inh}$ was 1.22×10^{-7} ($< 1.0 \times 10^{-6}$). The order of $ILCR_{inh}$ was men (1.53×10^{-7}) >
464 women (1.43×10^{-7}) > children (6.95×10^{-8}), and the risk for men was about twice that of children, but was
465 lower in women than in men. This may be caused by the fact that the inhalation and metabolic rate of
466 women are weaker than men (Bai et al., 2020). The highest average value was found in Shanghai, where
467 the average $ILCR_{ing}$ for the three groups were 1.72×10^{-6} , 1.62×10^{-6} , and 7.84×10^{-7} , respectively. Han et
468 al. (2020) found cases of excess cancer due to exposure to PAHs in large cities such as Shanghai. Only
469 1.6% of the three groups had $ILCR_{ing}$ higher than 1×10^{-6} , indicating that the health risks from inhalation
470 exposure were low. A similar conclusion was mentioned in an earlier review (Yan et al., 2019).

471 For dermal contact exposure, the average $ILCR_{der}$ was 1.04×10^{-6} ($> 1.0 \times 10^{-6}$). Compared to the
472 $ILCR_{inh}$, the health risk to adults was slightly higher than that to children, but women had higher risk
473 values than men. This may be caused by the fact that the body weight of women is weaker than men. The
474 order of $ILCR_{der}$ was women (1.32×10^{-6}) > men (1.15×10^{-6}) > children (6.33×10^{-6}), which is similar to
475 the results of previous studies (Bai et al., 2020). Among the three groups, 27.4% of the $ILCR_{der}$ values
476 were higher than 1×10^{-6} , and 0.7% were higher than 1×10^{-5} . This shows that there is a greater potential
477 carcinogenic risk through dermal contact exposure.

478 5 Discussion

479 It should be noted that model results have some uncertainties even though our model simulated the
480 main features of PAHs concentrations reasonably well. Firstly, we simulated lower BaP concentrations
481 when using the PKU inventory than when using the EDGAR inventory over most continental areas,
482 except for Inner Mongolia, eastern Russia, and north China (Fig. S6). The difference can be as high as
483 0.5 ng m^{-3} over some areas in wintertime although the spatial and temporal distributions are consistent.
484 The emission inventory remains to be constrained by more observations. Current observations are too
485 sparse to conduct detailed evaluation in areas where long-term measurements are not available. Secondly,
486 we tested the influence of heterogeneous reaction schemes on simulation. When heterogeneous reactions
487 were not considered, the model significantly overestimated the concentration of BaP (Fig. S7), suggesting
488 the importance of heterogeneous loss of BaP. Using the Langmuir-Hinshelwood mechanism, we
489 simulated lower concentrations in most regions of the northern hemisphere, especially in winter (Fig.



490 S8). However, the difference between the simulated results of the two mechanisms is significantly
491 reduced in summer due to high temperature and high humidity. This is consistent with the results by Mu
492 et al. (2018), i.e., low temperature and low humidity can significantly increase the lifetime of BaP.
493 Comparison of model results using different schemes and model intercomparison would further help
494 identify the uncertainties and improve model performance.

495 **6 Conclusion**

496 In this study, the PAHs modules were coupled into the IAP-AACM model to investigate the global
497 and regional distribution of PAHs. The model has the state-of -the-art heterogeneous mechanism and
498 allows us to consistently examine the multi-scale distribution of PAHs. Comparison with observations
499 shows that the model can reproduce the different concentrations of BaP at the stations in Asia, Europe,
500 the United States, and Canada. The model can capture the seasonal variation of BaP, with lower
501 concentrations in summer and higher concentrations in winter over the continents in the northern
502 hemisphere. The global distributions of BaP in 2013 and 2018 were very similar, with high concentrations
503 concentrated in eastern China and central Europe, even exceeding EU limits (1 ng m^{-3}). Compared with
504 2013, BaP concentration in 2018 showed a decrease in the United States, Poland, France, Czech, and
505 some regions in China. By contrast, the concentrations increased by $>10\%$ in India and South Africa.
506 Populations in these regions are facing increased health risks posed by PAHs.

507 In China, the decline in BTH (8.5%) and YRH (9.4%) benefitted from “the Action Plan”. However,
508 the decline was significantly less than that of conventional pollutants, such as $\text{PM}_{2.5}$. Changes in
509 meteorological conditions had a significant influence on changes in BaP concentration, which increased
510 in the Sichuan Basin and central China even though the emissions over these areas decreased due to the
511 control measures. There was a slight decrease in total ILCR (TILCR) values in 2018 compared to 2013.
512 For the different exposure routes, the dermal contact was an order of magnitude higher than the inhalation
513 route. The TILCR for adults was greater than that for children. 29.2% of TILCR were higher than 1.0×10^{-6} ,
514 indicating that there are still potential cancer risks in China. More attention must be paid to the non-
515 traditional pollutant pollutants and strict but different control measures are necessary to reduce PAHs'
516 concentration and health risks.

517 In summary, our study developed an effective tool for simulating the global and regional



518 concentrations of BaP and other PAHs and quantified the health risks in China from 2013 to 2018. Model
519 analysis indicated that emission inventories and heterogeneous reactions can significantly affect the
520 simulated BaP concentrations. Accurate emissions and reasonable representation of heterogeneous
521 reactions would greatly reduce the gap between model results and observation. However, the current
522 observations are insufficient to fully evaluate and constrain the model. Especially, long-term observations
523 are needed in Asia, India, and Africa. These regions are still facing significant health risks. In addition,
524 monitoring in the background and remote regions (such as the Arctic) is necessary to quantify the long-
525 range transport of PAHs.

526

527 *Code and data availability.* The source code and their introduction of IAP-AACM can be found online
528 via Zenodo (<https://doi.org/10.5281/zenodo.12214119>). The simulated data can be found via Zenodo
529 (<https://doi.org/10.5281/zenodo.11595165>). All the observational data are provided in the supplement
530 and can be found via Zenodo (<https://doi.org/10.5281/zenodo.11595165>).

531

532 *Author contributions.* ZcW developed the model, prepared the input data, performed the simulations and
533 analysis, and wrote the paper with suggestions from all co-authors. XC supported the coding and
534 conceived the idea of the paper. XC and ZfW revised the paper and provided scientific guidance through
535 all research advances. JL, ZW, LW, HC, YL, MQ, XT, and QW modified the manuscript. WW supported
536 the emission data. YW, ZZ, and ZJ supported the data analysis. All listed authors have read and approved
537 the final manuscript.

538

539 *Competing interests.* The authors declare that they have no conflict of interest.

540

541 *Disclaimer.* Publisher's note: Copernicus Publications remains neutral about jurisdictional claims in
542 published maps and institutional affiliations.

543

544 *Acknowledgements.* We are particularly grateful to Prof. Oliver Wild at Lancaster University for his help
545 with improving the paper. We thank Prof. Alexey Gusev at EMEP for providing MSC-E results as a good
546 reference to test our model performance. We also thank the National Key Scientific and Technological



547 Infrastructure project “Earth System Science Numerical Simulator Facility” (EarthLab).

548

549 *Financial support.* This research has been supported by the National Key R&D Program of China (Grant

550 NO.2020YFA0607801), the National Natural Science Foundation of China (Grant NO. 42377105) and

551 the National Key Scientific and Technological Infrastructure project “Earth System Science Numerical

552 Simulator Facility”.



553 **References**

554 Aulinger, A., Matthias, V., Quante, M.: CMAQ simulations of the benzo(a)pyrene distribution over
555 Europe for 2000 and 2001, *Atmospheric Environment*, 43, 4078-4086,
556 <https://doi.org/10.1016/j.atmosenv.2009.04.058>, 2009.

557 Aulinger, A., Quante, M., Matthias, V.: Introducing a Partitioning Mechanism for PAHs into the
558 Community Multiscale Air Quality Modeling System and Its Application to Simulating the
559 Transport of Benzo(a)pyrene over Europe, *Journal of Applied Meteorology and Climatology*,
560 46, 1718-1730, <https://doi.org/10.1175/2007jamc1395.1>, 2007.

561 Baek, S. O., Field, R. A., Goldstone, M. E., Kirk, P. W., Lester, J. N., Perry, R.: A review of atmospheric
562 polycyclic aromatic-hydrocarbons-sources, fate and behavior, *Water Air and Soil Pollution*, 60,
563 279-300, <https://doi.org/10.1007/bf00282628>, 1991.

564 Bai, L., Chen, W. Y., He, Z. J., Sun, S. Y., Qin, J.: Pollution characteristics, sources and health risk
565 assessment of polycyclic aromatic hydrocarbons in PM_{2.5} in an office building in northern
566 areas, China, *Sustainable Cities and Society*, 53, 10, <https://doi.org/10.1016/j.scs.2019.101891>,
567 2020.

568 Bieser, J., Aulinger, A., Matthias, V., Quante, M.: Impact of Emission Reductions between 1980 and 2020
569 on Atmospheric Benzo (a) pyrene Concentrations over Europe, *Water Air and Soil Pollution*,
570 223, 1393-1414, <https://doi.org/10.1007/s11270-011-0953-z>, 2012.

571 Byun, D., Schere, K. L.: Review of the governing equations, computational algorithms, and other
572 components of the models-3 Community Multiscale Air Quality (CMAQ) modeling system,
573 *Applied Mechanics Reviews*, 59, 51-77, <https://doi.org/10.1115/1.2128636>, 2006.

574 Byun, D. W., Dennis, R.: DESIGN ARTIFACTS IN EULERIAN AIR-QUALITY MODELS -
575 EVALUATION OF THE EFFECTS OF LAYER THICKNESS AND VERTICAL PROFILE
576 CORRECTION ON SURFACE OZONE CONCENTRATIONS, *Atmospheric Environment*, 29,
577 105-126, [https://doi.org/10.1016/1352-2310\(94\)00225-a](https://doi.org/10.1016/1352-2310(94)00225-a), 1995.

578 Cao, X. H., Huo, S. L., Zhang, H. X., Zheng, J. Q., He, Z. S., Ma, C. Z., Song, S.: Source emissions and
579 climate change impacts on the multimedia transport and fate of persistent organic pollutants,
580 Chaohu watershed, eastern China, *Journal of Environmental Sciences*, 109, 15-25,
581 <https://doi.org/10.1016/j.jes.2021.02.028>, 2021.



- 582 Chen, H. S., Wang, Z. F., Li, J., Tang, X., Ge, B. Z., Wu, X. L., Wild, O., Carmichael, G. R.: GNAQPMS-
583 Hg v1.0, a global nested atmospheric mercury transport model: model description, evaluation
584 and application to trans-boundary transport of Chinese anthropogenic emissions, *Geoscientific
585 Model Development*, 8, 2857-2876, <https://doi.org/10.5194/gmd-8-2857-2015>, 2015.
- 586 Chen, S. C., Liao, C. M.: Health risk assessment on human exposed to environmental polycyclic aromatic
587 hydrocarbons pollution sources, *Science of the Total Environment*, 366, 112-123,
588 <https://doi.org/10.1016/j.scitotenv.2005.08.047>, 2006.
- 589 Chen, X. S., Wang, Z. F., Li, J., Yu, F. Q.: Development of a Regional Chemical Transport Model with
590 Size-Resolved Aerosol Microphysics and Its Application on Aerosol Number Concentration
591 Simulation over China, *Sola*, 10, 83-87, <https://doi.org/10.2151/sola.2014-017>, 2014.
- 592 Chen, X. S., Yu, F. Q., Yang, W. Y., Sun, Y. L., Chen, H. S., Du, W., Zhao, J., Wei, Y., Wei, L. F., Du, H.
593 Y., Wang, Z., Wu, Q. Z., Li, J., An, J. L., Wang, Z. F.: Global-regional nested simulation of
594 particle number concentration by combing microphysical processes with an evolving organic
595 aerosol module, *Atmospheric Chemistry and Physics*, 21, 9343-9366,
596 <https://doi.org/10.5194/acp-21-9343-2021>, 2021.
- 597 Crippa, M., Solazzo, E., Huang, G. L., Guizzardi, D., Koffi, E., Muntean, M., Schieberle, C., Friedrich,
598 R., Janssens-Maenhout, G.: High resolution temporal profiles in the Emissions Database for
599 Global Atmospheric Research, *Scientific Data*, 7, 17, [https://doi.org/10.1038/s41597-020-0462-
600 2](https://doi.org/10.1038/s41597-020-0462-2), 2020.
- 601 Dachs, J., Eisenreich, S. J.: Adsorption onto aerosol soot carbon dominates gas-particle partitioning of
602 polycyclic aromatic hydrocarbons, *Environmental Science & Technology*, 34, 3690-3697,
603 <https://doi.org/10.1021/es991201+>, 2000.
- 604 Dong, Z. S., Kong, Z. H., Dong, Z., Shang, L. Q., Zhang, R. Q., Xu, R. X., Li, X.: Air pollution prevention
605 in central China: Effects on particulate-bound PAHs from 2010 to 2018, *Journal of
606 Environmental Management*, 344, 11, <https://doi.org/10.1016/j.jenvman.2023.118555>, 2023.
- 607 Du, H. Y., Li, J., Chen, X. S., Wang, Z. F., Sun, Y. L., Fu, P. Q., Li, J. J., Gao, J., Wei, Y.: Modeling of
608 aerosol property evolution during winter haze episodes over a megacity cluster in northern
609 China: roles of regional transport and heterogeneous reactions of SO₂,
610 *Atmospheric Chemistry and Physics*, 19, 9351-9370, <https://doi.org/10.5194/acp-19-9351-2019>,



- 611 2019.
- 612 Efstathiou, C. I., Matejovičová, J., Bieser, J., Lammel, G.: Evaluation of gas-particle partitioning in a
613 regional air quality model for organic pollutants, *Atmospheric Chemistry and Physics*, 16,
614 15327-15345, <https://doi.org/10.5194/acp-16-15327-2016>, 2016.
- 615 Feng, Y. Y., Ning, M., Lei, Y., Sun, Y. M., Liu, W., Wang, J. N.: Defending blue sky in China:
616 Effectiveness of the "Air Pollution Prevention and Control Action Plan" on air quality
617 improvements from 2013 to 2017, *Journal of Environmental Management*, 252, 13,
618 <https://doi.org/10.1016/j.jenvman.2019.109603>, 2019.
- 619 Finlayson-Pitts, B. J., Pitts, J. N. *Chemistry of the Upper and Lower Atmosphere: Theory, Experiments,*
620 *and Applications*. 2000.
- 621 Friedman, C. L., Pierce, J. R., Selin, N. E.: Assessing the Influence of Secondary Organic versus Primary
622 Carbonaceous Aerosols on Long-Range Atmospheric Polycyclic Aromatic Hydrocarbon
623 Transport, *Environmental Science & Technology*, 48, 3293-3302,
624 <https://doi.org/10.1021/es405219r>, 2014.
- 625 Friedman, C. L., Selin, N. E.: Long-Range Atmospheric Transport of Polycyclic Aromatic Hydrocarbons:
626 A Global 3-D Model Analysis Including Evaluation of Arctic Sources, *Environmental Science*
627 *& Technology*, 46, 9501-9510, <https://doi.org/10.1021/es301904d>, 2012.
- 628 Galarneau, E., Makar, P. A., Zheng, Q., Narayan, J., Zhang, J., Moran, M. D., Bari, M. A., Pathela, S.,
629 Chen, A., Chlumsky, R.: PAH concentrations simulated with the AURAMS-PAH chemical
630 transport model over Canada and the USA, *Atmospheric Chemistry and Physics*, 14, 4065-4077,
631 <https://doi.org/10.5194/acp-14-4065-2014>, 2014.
- 632 Gusev, A., Ilyin, I., Rozovskaya, O., Shatalov, V., Travnikov, O., Strijkina I. Assessment of transboundary
633 pollution by toxic substances: Heavy metals and POPs, *Meteorological Synthesizing Centre -*
634 *East, Russia*, 74 pp., 2019.
- 635 Han, F. L., Guo, H., Hu, J. L., Zhang, J., Ying, Q., Zhang, H. L.: Sources and health risks of ambient
636 polycyclic aromatic hydrocarbons in China, *Science of the Total Environment*, 698, 13,
637 <https://doi.org/10.1016/j.scitotenv.2019.134229>, 2020.
- 638 Hansen, K. M., Christensen, J. H., Brandt, J., Frohn, L. M., Geels, C.: Modelling atmospheric transport
639 of α -hexachlorocyclohexane in the Northern Hemisphere with a 3-D dynamical model: DEHM-



- 640 POP, *Atmos. Chem. Phys.*, 4, 1125-1137, <https://doi.org/10.5194/acp-4-1125-2004>, 2004.
- 641 Haritash, A. K., Kaushik, C. P.: Biodegradation aspects of Polycyclic Aromatic Hydrocarbons (PAHs): A
642 review, *Journal of Hazardous Materials*, 169, 1-15,
643 <https://doi.org/10.1016/j.jhazmat.2009.03.137>, 2009.
- 644 Harner, T., Bidleman, T. F.: Octanol-air partition coefficient for describing particle/gas partitioning of
645 aromatic compounds in urban air, *Environmental Science & Technology*, 32, 1494-1502,
646 <https://doi.org/10.1021/es970890r>, 1998.
- 647 Inomata, Y., Kajino, M., Sato, K., Ohara, T., Kurokawa, J., Ueda, H., Tang, N., Hayakawa, K., Ohizumi,
648 T., Akimoto, H.: Source contribution analysis of surface particulate polycyclic aromatic
649 hydrocarbon concentrations in northeastern Asia by source-receptor relationships,
650 *Environmental Pollution*, 182, 324-334, <https://doi.org/10.1016/j.envpol.2013.07.020>, 2013.
- 651 Inomata, Y., Kajino, M., Sato, K., Ohara, T., Kurokawa, J. I., Ueda, H., Tang, N., Hayakawa, K., Ohizumi,
652 T., Akimoto, H.: Emission and Atmospheric Transport of Particulate PAHs in Northeast Asia,
653 *Environmental Science & Technology*, 46, 4941-4949, <https://doi.org/10.1021/es300391w>,
654 2012.
- 655 Jonker, M. T. O., Koelmans, A. A.: Sorption of polycyclic aromatic hydrocarbons and polychlorinated
656 biphenyls to soot and soot-like materials in the aqueous environment mechanistic considerations,
657 *Environmental Science & Technology*, 36, 3725-3734, <https://doi.org/10.1021/es020019x>, 2002.
- 658 Jury, W. A., Spencer, W. F., Farmer, W. J.: Behavior Assessment Model for Trace Organics in Soil: I.
659 Model Description, *Journal of Environmental Quality*, 12, 558-564,
660 <https://doi.org/10.2134/jeq1983.00472425001200040025x>, 1983.
- 661 Kahan, T. F., Kwamena, N. O. A., Donaldson, D. J.: Heterogeneous ozonation kinetics of polycyclic
662 aromatic hydrocarbons on organic films, *Atmospheric Environment*, 40, 3448-3459,
663 <https://doi.org/10.1016/j.atmosenv.2006.02.004>, 2006.
- 664 Karickhoff, S. W.: Semi-empirical estimation of sorption of hydrophobic pollutants on natural sediments
665 and soils, *Chemosphere*, 10, 833-846, [https://doi.org/10.1016/0045-6535\(81\)90083-7](https://doi.org/10.1016/0045-6535(81)90083-7), 1981.
- 666 Keyte, I. J., Harrison, R. M., Lammel, G.: Chemical reactivity and long-range transport potential of
667 polycyclic aromatic hydrocarbons - a review, *Chemical Society Reviews*, 42, 9333-9391,
668 <https://doi.org/10.1039/c3cs60147a>, 2013.



- 669 Klöpffer, W., Wagner, B., Scheringer, M.: Atmospheric degradation of organic substances data for
670 persistence and long-range transport potential, *Environmental Science and Pollution Research*
671 - International, 14, 143-144, <https://doi.org/10.1065/espr2007.04.408>, 2007.
- 672 Kwamena, N. O. A., Clarke, J. P., Kahan, T. F., Diamond, M. L., Donaldson, D. J.: Assessing the
673 importance of heterogeneous reactions of polycyclic aromatic hydrocarbons in the urban
674 atmosphere using the Multimedia Urban Model, *Atmospheric Environment*, 41, 37-50,
675 <https://doi.org/10.1016/j.atmosenv.2006.08.016>, 2007.
- 676 Lammel, G., Dvorská, A., Klánová, J., Kohoutek, J., Kukacka, P., Prokes, R., Sehili, A. M.: Long-range
677 Atmospheric Transport of Polycyclic Aromatic Hydrocarbons is Worldwide Problem - Results
678 from Measurements at Remote Sites and Modelling, *Acta Chimica Slovenica*, 62, 729-735, 2015.
- 679 Lammel, G., Sehili, A. M.: Global fate and distribution of polycyclic aromatic hydrocarbons emitted from
680 Europe and Russia, *Atmospheric Environment*, 41, 8301-8315,
681 <https://doi.org/10.1016/j.atmosenv.2007.06.050>, 2007.
- 682 Lammel, G., Sehili, A. M., Bond, T. C., Feichter, J., Grassl, H.: Gas/particle partitioning and global
683 distribution of polycyclic aromatic hydrocarbons--a modelling approach, *Chemosphere*, 76, 98-
684 106, <https://doi.org/10.1016/j.chemosphere.2009.02.017>, 2009.
- 685 Li, J., Wang, Z. F., Zhuang, G., Luo, G., Sun, Y., Wang, Q.: Mixing of Asian mineral dust with
686 anthropogenic pollutants over East Asia: a model case study of a super-duststorm in March 2010,
687 *Atmospheric Chemistry and Physics*, 12, 7591-7607, <https://doi.org/10.5194/acp-12-7591-2012>,
688 2012.
- 689 Li, R. F., Zhang, J., Krebs, P.: Global trade drives transboundary transfer of the health impacts of
690 polycyclic aromatic hydrocarbon emissions, *Communications Earth & Environment*, 3, 13,
691 <https://doi.org/10.1038/s43247-022-00500-y>, 2022.
- 692 Li, Z., Mulholland, J. A., Romanoff, L. C., Pittman, E. N., Trinidad, D. A., Lewin, M. D., Sjödin, A.:
693 Assessment of non-occupational exposure to polycyclic aromatic hydrocarbons through
694 personal air sampling and urinary biomonitoring, *Journal of Environmental Monitoring*, 12,
695 1110-1118, <https://doi.org/10.1039/c000689k>, 2010.
- 696 Lin, Y., Ma, Y. Q., Qiu, X. H., Li, R., Fang, Y. H., Wang, J. X., Zhu, Y. F., Hu, D.: Sources, transformation,
697 and health implications of PAHs and their nitrated, hydroxylated, and oxygenated derivatives in



- 698 PM2.5 in Beijing, *Journal of Geophysical Research-Atmospheres*, 120, 7219-7228,
699 <https://doi.org/10.1002/2015jd023628>, 2015.
- 700 Liu, S. J., Lu, Y. L., Wang, T. Y., Xie, S. W., Jones, K. C., Sweetman, A. J.: Using gridded multimedia
701 model to simulate spatial fate of Benzo α pyrene on regional scale, *Environment International*,
702 63, 53-63, <https://doi.org/10.1016/j.envint.2013.10.015>, 2014.
- 703 Lou, S. J., Shrivastava, M., Ding, A. J., Easter, R. C., Fast, J. D., Rasch, P. J., Shen, H. Z., Simonich, S.
704 M., Smith, S. J., Tao, S., Zelenyuk, A.: Shift in Peaks of PAH-Associated Health Risks From
705 East Asia to South Asia and Africa in the Future, *Earths Future*, 11, 15,
706 <https://doi.org/10.1029/2022ef003185>, 2023.
- 707 Ma, W. L., Liu, L. Y., Jia, H. L., Yang, M., Li, Y. F.: PAHs in Chinese atmosphere Part I: Concentration,
708 source and temperature dependence, *Atmospheric Environment*, 173, 330-337,
709 <https://doi.org/10.1016/j.atmosenv.2017.11.029>, 2018.
- 710 Ma, W. L., Zhu, F. J., Liu, L. Y., Jia, H. L., Yang, M., Li, Y. F.: PAHs in Chinese atmosphere Part II: Health
711 risk assessment, *Ecotoxicology and Environmental Safety*, 200, 9,
712 <https://doi.org/10.1016/j.ecoenv.2020.110774>, 2020.
- 713 Mu, Q., Shiraiwa, M., Octaviani, M., Ma, N., Ding, A. J., Su, H., Lammel, G., Pöschl, U., Cheng, Y. F.:
714 Temperature effect on phase state and reactivity controls atmospheric multiphase chemistry and
715 transport of PAHs, *Science Advances*, 4, 8, <https://doi.org/10.1126/sciadv.aap7314>, 2018.
- 716 Nam, K. J., Li, Q., Heo, S. K., Tariq, S., Loy-Benitez, J., Woo, T. Y., Yoo, C. K.: Inter-regional multimedia
717 fate analysis of PAHs and potential risk assessment by integrating deep learning and climate
718 change scenarios, *Journal of Hazardous Materials*, 411, 12,
719 <https://doi.org/10.1016/j.jhazmat.2021.125149>, 2021.
- 720 Octaviani, M., Tost, H., Lammel, G.: Global simulation of semivolatile organic compounds - development
721 and evaluation of the MESSy submodel SVOC (v1.0), *Geoscientific Model Development*, 12,
722 3585-3607, <https://doi.org/10.5194/gmd-12-3585-2019>, 2019.
- 723 Odabasi, M., Cetin, E., Sofuoglu, A.: Determination of octanol-air partition coefficients and supercooled
724 liquid vapor pressures of PAHs as a function of temperature: Application to gas-particle
725 partitioning in an urban atmosphere, *Atmospheric Environment*, 40, 6615-6625,
726 <https://doi.org/10.1016/j.atmosenv.2006.05.051>, 2006.



- 727 Quan, J. N., Tie, X. X., Zhang, Q., Liu, Q., Li, X., Gao, Y., Zhao, D. L.: Characteristics of heavy aerosol
728 pollution during the 2012-2013 winter in Beijing, China, *Atmospheric Environment*, 88, 83-89,
729 <https://doi.org/10.1016/j.atmosenv.2014.01.058>, 2014.
- 730 Ravindra, K., Sokhi, R., Van Grieken, R.: Atmospheric polycyclic aromatic hydrocarbons: Source
731 attribution, emission factors and regulation, *Atmospheric Environment*, 42, 2895-2921,
732 <https://doi.org/10.1016/j.atmosenv.2007.12.010>, 2008.
- 733 San José, R., Pérez, J. L., Callén, M. S., López, J. M., Mastral, A.: BaP (PAH) air quality modelling
734 exercise over Zaragoza (Spain) using an adapted version of WRF-CMAQ model,
735 *Environmental Pollution*, 183, 151-158, <https://doi.org/10.1016/j.envpol.2013.02.025>, 2013.
- 736 Seigneur, C., Karamchandani, P., Lohman, K., Vijayaraghavan, K., Shia, R. L.: Multiscale modeling of
737 the atmospheric fate and transport of mercury, *Journal of Geophysical Research-Atmospheres*,
738 106, 27795-27809, <https://doi.org/10.1029/2000jd000273>, 2001.
- 739 Semeena, V. S., Lammel, G.: The significance of the grasshopper effect on the atmospheric distribution
740 of persistent organic substances, *Geophysical Research Letters*, 32, 5,
741 <https://doi.org/10.1029/2004gl022229>, 2005.
- 742 Shen, H. Z., Tao, S., Liu, J. F., Huang, Y., Chen, H., Li, W., Zhang, Y. Y., Chen, Y. C., Su, S., Lin, N., Xu,
743 Y. Y., Li, B. G., Wang, X. L., Liu, W. X.: Global lung cancer risk from PAH exposure highly
744 depends on emission sources and individual susceptibility, *Scientific Reports*, 4, 8,
745 <https://doi.org/10.1038/srep06561>, 2014.
- 746 Shrivastava, M., Lou, S., Zelenyuk, A., Easter, R. C., Corley, R. A., Thrall, B. D., Rasch, P. J., Fast, J. D.,
747 Simonich, S. L. M., Shen, H. Z., Tao, S.: Global long-range transport and lung cancer risk from
748 polycyclic aromatic hydrocarbons shielded by coatings of organic aerosol, *Proceedings of the*
749 *National Academy of Sciences of the United States of America*, 114, 1246-1251,
750 <https://doi.org/10.1073/pnas.1618475114>, 2017.
- 751 Skamarock, W. C., Klemp, J. B., Dudhia, J., Gill, D., Barker, D. M., Duda, M. G., Huang, X.-Y., Wang,
752 W., Powers, J. G. A Description of the Advanced Research WRF Version 3. 2008.
- 753 Smith, R. L., Davis, J. M., Speckman, P.: Assessing the human health risk of atmospheric particles,
754 *Novartis Found Symp*, 220, 59-72; discussion 72-9,
755 <https://doi.org/10.1002/9780470515600.ch4>, 1999.



- 756 Stockwell, W. R., Middleton, P., Chang, J. S., Tang, X. Y.: The Second Generation Regional Acid
757 Deposition Model Chemical Mechanism for Regional Air Quality Modeling, *Journal of*
758 *Geophysical Research-Atmospheres*, 95, 16343-16367,
759 <https://doi.org/10.1029/JD095iD10p16343>, 1990.
- 760 Strand, A., Hov, O.: A model strategy for the simulation of chlorinated hydrocarbon distributions in the
761 global environment, *Water Air and Soil Pollution*, 86, 283-316,
762 <https://doi.org/10.1007/bf00279163>, 1996.
- 763 Su, C., Zheng, D. F., Zhang, H., Liang, R. Y.: The past 40 years' assessment of urban-rural differences in
764 Benzo a pyrene contamination and human health risk in coastal China, *Science of the Total*
765 *Environment*, 901, 9, <https://doi.org/10.1016/j.scitotenv.2023.165993>, 2023.
- 766 van Noort, P. C. M.: A thermodynamics-based estimation model for adsorption of organic compounds by
767 carbonaceous materials in environmental sorbents, *Environmental Toxicology and Chemistry*,
768 22, 1179-1188, 2003.
- 769 Walcek, C. J., Aleksic, N. M.: A simple but accurate mass conservative, peak-preserving, mixing ratio
770 bounded advection algorithm with Fortran code, *Atmospheric Environment*, 32, 3863-3880,
771 [https://doi.org/10.1016/s1352-2310\(98\)00099-5](https://doi.org/10.1016/s1352-2310(98)00099-5), 1998.
- 772 Wang, L., Zhang, F. Y., Pilot, E., Yu, J., Nie, C. J., Holdaway, J., Yang, L. S., Li, Y. H., Wang, W. Y.,
773 Vardoulakis, S., Krafft, T.: Taking Action on Air Pollution Control in the Beijing-Tianjin-Hebei
774 (BTH) Region: Progress, Challenges and Opportunities, *International Journal of Environmental*
775 *Research and Public Health*, 15, 27, <https://doi.org/10.3390/ijerph15020306>, 2018.
- 776 Wang, Y. S., Li, W. J., Gao, W. K., Liu, Z. R., Tian, S. L., Shen, R. R., Ji, D. S., Wang, S., Wang, L. L.,
777 Tang, G. Q., Song, T., Cheng, M. T., Wang, G. H., Gong, Z. Y., Hao, J. M., Zhang, Y. H.: Trends
778 in particulate matter and its chemical compositions in China from 2013-2017, *Science China-*
779 *Earth Sciences*, 62, 1857-1871, <https://doi.org/10.1007/s11430-018-9373-1>, 2019.
- 780 Wang, Z. F., Maeda, T., Hayashi, M., Hsiao, L. F., Liu, K. Y.: A nested air quality prediction modeling
781 system for urban and regional scales: Application for high-ozone episode in Taiwan, *Water Air*
782 *and Soil Pollution*, 130, 391-396, <https://doi.org/10.1023/a:1013833217916>, 2001.
- 783 Wang, Z. X., Li, J. X., Mu, X., Zhao, L. Y., Gu, C., Gao, H., Ma, J. M., Mao, X. X., Huang, T.: A WRF-
784 CMAQ modeling of atmospheric PAH cycling and health risks in the heavy petrochemical



- 785 industrialized Lanzhou valley, Northwest China, *Journal of Cleaner Production*, 291, 9,
786 <https://doi.org/10.1016/j.jclepro.2021.125989>, 2021.
- 787 Wei, Y., Chen, X. S., Chen, H. S., Li, J., Wang, Z. F., Yang, W. Y., Ge, B. Z., Du, H. Y., Hao, J. Q., Wang,
788 W., Li, J. J., Sun, Y. L., Huang, H. L.: IAP-AACM v1.0: a global to regional evaluation of the
789 atmospheric chemistry model in CAS-ESM, *Atmospheric Chemistry and Physics*, 19, 8269-
790 8296, <https://doi.org/10.5194/acp-19-8269-2019>, 2019.
- 791 Wu, Z. C., Chen, X. S., and Wang, Z. F.: A Global-Regional Nested Model of Polycyclic aromatic
792 hydrocarbons, Zenodo [code], <https://doi.org/10.5281/zenodo.12214119>, 2024.
- 793 Wu, Z. C., Chen, X. S., and Wang, Z. F.: Results and validation of Global-Regional Nested Model for
794 polycyclic aromatic hydrocarbons., Zenodo [data set],
795 <https://doi.org/10.5281/zenodo.11595165>, 2024.
- 796 Yan, D. H., Wu, S. H., Zhou, S. L., Tong, G. J., Li, F. F., Wang, Y. M., Li, B. J.: Characteristics, sources
797 and health risk assessment of airborne particulate PAHs in Chinese cities: A review,
798 *Environmental Pollution*, 248, 804-814, <https://doi.org/10.1016/j.envpol.2019.02.068>, 2019.
- 799 Ye, Q., Li, J., Chen, X., Chen, H., Yang, W., Du, H., Pan, X., Tang, X., Wang, W., Zhu, L., Li, J., Wang,
800 Z., Wang, Z.: High-resolution modeling of the distribution of surface air pollutants and their
801 intercontinental transport by a global tropospheric atmospheric chemistry source-receptor
802 model (GNAQPMS-SM), *Geoscientific Model Development*, 14, 7573-7604,
803 <https://doi.org/10.5194/gmd-14-7573-2021>, 2021.
- 804 Zaveri, R. A., Peters, L. K.: A new lumped structure photochemical mechanism for large-scale
805 applications, *Journal of Geophysical Research-Atmospheres*, 104, 30387-30415,
806 <https://doi.org/10.1029/1999jd900876>, 1999.
- 807 Zhang, L., Brook, J. R., Vet, R.: A revised parameterization for gaseous dry deposition in air-quality
808 models, *Atmospheric Chemistry and Physics*, 3, 2067-2082, [https://doi.org/10.5194/acp-3-](https://doi.org/10.5194/acp-3-2067-2003)
809 2067-2003, 2003.
- 810 Zhang, M., Xie, J. F., Wang, Z. T., Zhao, L. J., Zhang, H., Li, M.: Determination and source identification
811 of priority polycyclic aromatic hydrocarbons in PM_{2.5} in Taiyuan, China, *Atmospheric
812 Research*, 178, 401-414, <https://doi.org/10.1016/j.atmosres.2016.04.005>, 2016.
- 813 Zhang, Q., Zheng, Y. X., Tong, D., Shao, M., Wang, S. X., Zhang, Y. H., Xu, X. D., Wang, J. N., He, H.,



- 814 Liu, W. Q., Ding, Y. H., Lei, Y., Li, J. H., Wang, Z. F., Zhang, X. Y., Wang, Y. S., Cheng, J., Liu,
815 Y., Shi, Q. R., Yan, L., Geng, G. N., Hong, C. P., Li, M., Liu, F., Zheng, B., Cao, J. J., Ding, A.
816 J., Gao, J., Fu, Q. Y., Huo, J. T., Liu, B. X., Liu, Z. R., Yang, F. M., He, K. B., Hao, J. M.: Drivers
817 of improved PM_{2.5} air quality in China from 2013 to 2017, *Proceedings of the National*
818 *Academy of Sciences of the United States of America*, 116, 24463-24469,
819 <https://doi.org/10.1073/pnas.1907956116>, 2019.
- 820 Zhang, Y., Hemperly, J., Meskhidze, N., Skamarock, W. C.: The Global Weather Research and
821 Forecasting (GWRP) Model: Model Evaluation, Sensitivity Study, and Future Year Simulation,
822 *Atmospheric and Climate Sciences*, 2, 231-253, <https://doi.org/10.4236/acs.2012.23024>, 2012a.
- 823 Zhang, Y., Jaeglé, L., van Donkelaar, A., Martin, R. V., Holmes, C. D., Amos, H. M., Wang, Q., Talbot,
824 R., Artz, R., Brooks, S., Luke, W., Holsen, T. M., Felton, D., Miller, E. K., Perry, K. D., Schmelz,
825 D., Steffen, A., Tordon, R., Weiss-Penzias, P., Zsolway, R.: Nested-grid simulation of mercury
826 over North America, *Atmospheric Chemistry and Physics*, 12, 6095-6111,
827 <https://doi.org/10.5194/acp-12-6095-2012>, 2012b.
- 828 Zhang, Y., Shen, H., Tao, S., Ma, J.: Modeling the atmospheric transport and outflow of polycyclic
829 aromatic hydrocarbons emitted from China, *Atmospheric Environment*, 45, 2820-2827,
830 <https://doi.org/10.1016/j.atmosenv.2011.03.006>, 2011a.
- 831 Zhang, Y., Tao, S., Ma, J., Simonich, S.: Transpacific transport of benzo[a]pyrene emitted from Asia,
832 *Atmospheric Chemistry and Physics*, 11, 11993-12006, [https://doi.org/10.5194/acp-11-11993-](https://doi.org/10.5194/acp-11-11993-2011)
833 2011, 2011b.
- 834 Zhang, Y. X., Tao, S.: Global atmospheric emission inventory of polycyclic aromatic hydrocarbons (PAHs)
835 for 2004, *Atmospheric Environment*, 43, 812-819,
836 <https://doi.org/10.1016/j.atmosenv.2008.10.050>, 2009.
- 837 Zhang, Y. X., Tao, S., Shen, H. Z., Ma, J. M.: Inhalation exposure to ambient polycyclic aromatic
838 hydrocarbons and lung cancer risk of Chinese population, *Proceedings of the National Academy*
839 *of Sciences of the United States of America*, 106, 21063-21067,
840 <https://doi.org/10.1073/pnas.0905756106>, 2009.
- 841 Zhen, Z. X.: Observation and simulation of atmospheric polycyclic aromatic hydrocarbons in the North
842 China Plain, Ph.D.thesis, Nanjing university of information science and technology, China, 142



843 pp., 2023.

844 Zhu, F. J., Ma, W. L., Hu, P. T., Zhang, Z. F., Li, Y. F.: Temporal trends of atmospheric PAHs: Implications

845 for the influence of the clean air action, *Journal of Cleaner Production*, 296, 8,

846 <https://doi.org/10.1016/j.jclepro.2021.126494>, 2021.